Journal of Molecular Structure 1202 (2020) 127226

Contents lists available at ScienceDirect

Journal of Molecular Structure

journal homepage: http://www.elsevier.com/locate/molstruc

Experimental and theoretical probing of the physicochemical properties of ionic liquids composed of [Bn-DBU]$^+$ cation and various anions

Sara Fallah Ghasemi Gildeh, Hossein Roohi*, Morteza Mehrdad, Kurosh Rad-Moghadam, Khatereh Ghauri

Department of Chemistry, Faculty of Science, University of Guilan, Rasht, Iran

ARTICLE INFO

Article history:
Received 10 May 2019
Received in revised form
11 October 2019
Accepted 13 October 2019
Available online 18 October 2019

Keywords:
Bn-DBU
M06−2X
HNMR
FTIR
TGA
MESP

ABSTRACT

The experimental approaches coupled with computational methods are powerful tools to understand the physicochemical properties of ionic liquids. The 1,8-diazobicyclo[5.4.0]undec-7-ene-8-benzylium ([Bn-DBU]$^+$) cation is a N-substituted DBU cation that was joined with various anions for production of [Bn-DBU][Y_{1-8}], (Y_{1-8} = $CH_3CO_2^-$, $PhSO_2^-$, $PhSO_3^-$, HCO_3^-, HSO_4^-, $CF_3CO_2^-$, BF_4^-, and SCN^-) ionic liquids (ILs). In this study, at first, several aprotic ionic liquids composed of [Bn-DBU]$^+$ cation and various anions were synthesized and characterized experimentally by the combined of ^{1}HNMR and FTIR spectroscopies, and thermogravimetric analysis (TGA). Then, density functional theory (DFT) at M06−2X/6−311++G(d,p) level of theory was used for calculation of the molecular electrostatic potential (MESP), interaction energies, structural parameters, vibrational frequencies, topological properties, charge transfer (CT) values and non-covalent interaction index.

1. Introduction

Ionic liquids (ILs) are a fascinating class of low melting salts that generally are composed of large unsymmetrical organic cation and a weakly-coordinating inorganic or organic anion [1−3]. They exhibit excellent physiochemical properties such as low melting point, vanishing vapor pressure, non−flammability, favorable solvation behavior, resistant to oxidation and extraordinary high thermal and electrochemical stability in the presence of air and moisture, in contrast to the characteristics of traditional volatile organic solvents and they can be a suitable replacement for traditional toxic solvents in organic synthesis [4−16].

The 1,8-diazobicyclo[5.4.0]undec-7-ene (DBU) is an amidine strong organic base having amidino functional group [17,18] that has been extensively applied in the base-induced reactions with excellent catalytic activity. However, the separation of DBU from the products mixture is generally difficult. The functionalized ionic liquids and task-specific ionic liquids (TSILs) with special functions can overcome this drawback and exhibit the similar basicity to DBU accompanied with the general features of ILs [19].

The study of the various properties of N-substituted DBU-based ionic liquids proved the advantages and uniqueness of these ILs as catalyst and a non-nucleophilic base in different organic reactions such as Knoevenagel condensation reaction, aza-Michael addition reaction, etc [19−24]. Because of the unique properties DBU-based ionic liquids such as polarity, conductivity, solubilizing power and viscosity, the ILs can be used as switchable polarity solvents (SPS) [25−30]. Thus, the tunable behavior of the properties of DBU-based ionic liquids can be employed for a number of applications ranging from CO_2 capturing [25,26,31] to dissolution of biopolymers [32]. This type of the ILs can also be used for a variety of purposes such as extraction [33] and thermally-stable lubricants [34].

One of the most attractive characters of DBU-based ionic liquids is that their properties can change with the combination of different anions and various substituents (aromatic or aliphatic alkyl chains groups) which can be linked to DBU rings of their cation, which provides the chances for designing and developing DBU-based ionic liquids with excellent properties [29,35,36]. Wu et al., in 2014 first synthesized several DBU-based ILs ([Et−DBU][$PHSO_3$], [Al−DBU][$PhSO_3$], [Bu−DBU][$PhSO_3$] and [Bn−DBU][$PhSO_3$]) and used as solvents in the dehydration of glucose to 5-

* Corresponding author.
E-mail addresses: hrouhi@gmail.com, hroohi@guilan.ac.ir (H. Roohi).

https://doi.org/10.1016/j.molstruc.2019.127226
0022-2860/

hydroxymethylfurfural (HMF) [37].

In the first part of this work, we attempt to report the synthesis, spectroscopic characterization and thermal stability of DBU based ILs including various anions ($CH_3CO_2^-$, $PhSO_2^-$, $PhSO_3^-$, HCO_3^-, HSO_4^-, $CF_3CO_2^-$, BF_4^- and SCN^-) and 1,8-diazobicyclo[5.4.0]undec-7-ene-8-benzylium ($[Bn-DBU]^+$) cation.

An increase in the computational power and availability of computational resources has resulted in an increase of publications that use quantum chemical methods to offer theoretical underpinning to experimental data and prediction of physicochemical properties of ionic liquids [38–44]. To the best our knowledge interaction between [Bn−DBU]-based cation and above anions has not been characterized and no detailed studies exist on the influence of different anions on hydrogen bonding strength between their constituents. In the second part of the present work, interaction energy between the $[Bn-DBU]^+$ cation and the anions, geometrical parameters and topological properties, electrochemical and thermal stability of $[X][Y_{1\text{-}8}]$, ($[X]^+ = [Bn-DBU]^+$, and $Y_{1\text{-}8} = CH_3CO_2^-$, $PhSO_2^-$, $PhSO_3^-$, HCO_3^-, HSO_4^-, $CF_3CO_2^-$, BF_4^- and SCN^-) ILs based on experimental and theoretical methods were explored. An overview of ionic liquids studied in this work is shown in Fig. 1.

2. Experimental methods

2.1. Material

Chemicals were purchased from Merck and Aldrich chemical companies (purity > 97%) and were used without further purification.

2.2. Synthesis of the ILs, [Bn-DBU][Y]

The ionic liquids were prepared *via* anion exchange from the pre-synthesized [Bn-DBU]Cl salt. To synthesize the salt, DBU (0.5 mol) and benzyl bromide (0.8 mol) were added to a flask (1 L) containing ethyl acetate (500 mL) and a magnetic stirring bar. The reaction mixture was stirred at room temperature for 48 h, during which the solution was separated into two phases. The supernatant ethyl acetate phase was separated off and the ionic liquid phase was washed with diethyl ether (3 × 25 mL) to remove the unreacted starting materials. The remaining solvent was evaporated under vacuum, to yield the salt [Bn-DBU]Cl. To derive the other ILs, [Bn-DBU]Cl (0.3 mol) and NaY (Y = $CH_3CO_2^-$, $PhSO_2^-$, HCO_3^-, $CF_3CO_2^-$, BF_4^-, or SCN^-) in slight excess amount (0.35 mol) were added to acetonitrile (800 mL) in a beaker (1 L) equipped with a magnetic stirring bar. The mixture was stirred at room temperature for about 48 h. Afterward, the solids were removed by centrifugation and the liquid phase was heated at 80 °C under vacuum to evaporate acetonitrile and to get the ILs. Accordingly, six Bn-DBU based ILs including [Bn-DBU][CH_3CO_2], [Bn-DBU][$PhSO_2$], [Bn-DBU][HCO_3], [Bn-DBU][CF_3CO_2], [Bn-DBU][BF_4] and [Bn-DBU][SCN] were synthesized (Fig. 2). This synthetic method gave the [Bn-DBU]-based ionic liquids in 94–96% yields. Fig. 3 shows images of the synthesized Bn-DBU-based ionic liquid.

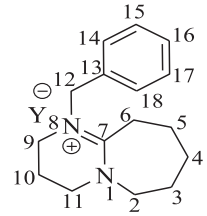

$Y = CH_3CO_2$, $PhSO_2$, HCO_3, CF_3CO_2, BF_4, SCN

Fig. 1. Overview of DBU based ionic liquids.

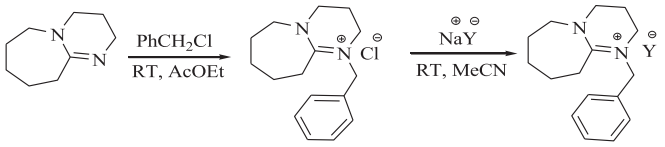

$Y = CH3CO_2^-$, $PhSO_2^-$, HCO_3^-, $CF_3CO_2^-$, BF_4^-, SCN^-

Fig. 2. Preparation of DBU-based ILs, [Bn−DBU][CH_3CO_2], [Bn−DBU][$PhSO_2$], [Bn−DBU][HCO_3], [Bn−DBU][CF_3CO_2], [Bn−DBU][BF_4] and [Bn−DBU][SCN] ILs.

2.3. Characterization

The structure of the ILs was confirmed based on the ^1H NMR and FT-IR spectral data of the samples. The NMR spectra were recorded on a Bruker (DRX400 MHz Advance, Germany) spectrometer and the FT-IR spectra were obtained from net samples coated on KBr discs by a Bruker (VERTEX 70, Germany) spectrometer.

2.4. Thermogravimetric analyses

To determine the thermal properties of the synthesized ionic liquids, thermogravimetric analysis (TGA) were performed on a DSC-TG analyzer (Q 600, TA company, America). Samples were heated from 50 to 600 °C under N_2 atmosphere at ramp of 20 °C min^{-1} with the flux 60 mL min^{-1}.

3. Computational detail

Density functional theory (DFT) was used to predict the geometrical structure, energetic and electronic properties and characterization of the nature of intermolecular interactions of ionic liquids. Geometry optimizations and calculation of the property of the ionic liquids were carried out at M06−2X/6−311++G(d,p) level [45–47]. The counterpoise method (CP) [48] was used to correct for basis set superposition error (BSSE) in the calculation of interaction energies. Also, dispersion correction on the interaction energies by M06-2X-D3 functional was explored. To characterize the stationary points and calculation of zero-point vibrational energy (ZPVE) as well as thermochemical quantities, vibrational frequency analysis were performed at mentioned level of theory. In addition to electronic interaction energy, interaction enthalpy (ΔH) and free energy (ΔG) of the ILs at 298.15 K were calculated. All the above calculations were performed by using Gaussian program [49].

The electronic distribution in a molecule can be explored employing the molecular electrostatic potential (MESP) topography analysis. The electrostatic potential $V(\mathbf{r})$ is a three-dimensional local property that can be evaluated at any or all points $\mathbf{r}$ in the space of a system by $V(r) = \sum_A \frac{Z_A}{|\mathbf{R_A}-\mathbf{r}|} - \int \frac{\rho(\mathbf{r}')d\mathbf{r}'}{|\mathbf{r}'-\mathbf{r}|}$ in terms of atomic units, au. The Z_A is the charge on nucleus A, located at $\mathbf{R_A}$; $|\mathbf{R_A}-\mathbf{r}|$ represents its distance from r, just as $|\mathbf{r'}-\mathbf{r}|$ is the distance of each electronic charge increment $-e\rho(\mathbf{r'})d\mathbf{r'}$ from $\mathbf{r}$. $V(\mathbf{r})$ may be either positive or negative in any given region, depending upon whether the effect of the nuclei or the electrons is dominant there [50]. The MESPs on the 0.001 au contours were calculated at the M06−2X/6−311++G(d,p) level using the Multiwfn program [51].

The NBO analysis [52] was carried out using version 3.1 of NBO package [53] and topological properties of electron charge density were also performed by the AIM2000 program package [54] at M06−2X/6−311++G(d,p) level of theory. The energy decomposition analysis (EDA) was performed by Amsterdam Density

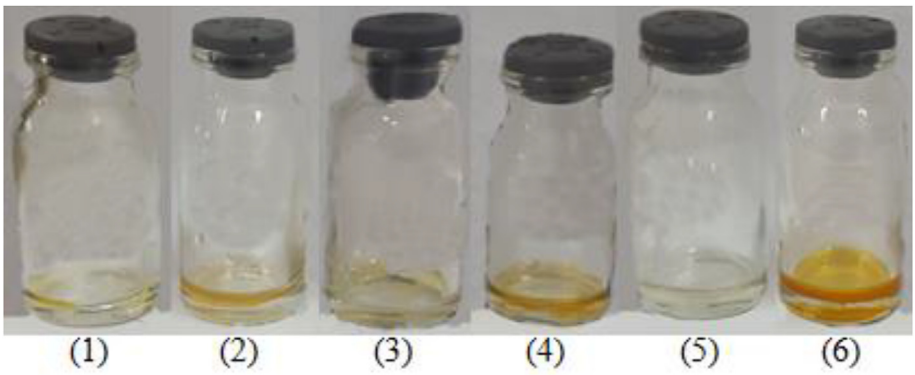

Fig. 3. The six synthesized DBU-based ILs, (1) [Bn−DBU][CH_3CO_2], (2) [Bn−DBU][$PhSO_2$], (3) [Bn−DBU][HCO_3], (4) [Bn−DBU][CF_3CO_2], (5) [Bn−DBU][BF_4] and (6) [Bn−DBU][SCN].

Functional theory (ADF) (2010.01) software [55–57] to understand the nature of interaction between cations and anions of the ILs at the PB86-D3/TZP level of theory.

The Non-Covalent Interactions, NCI, index based on the electron density and its derivatives was used for characterization of the intermolecular interactions [58,59]. In this work, we used Multiwfn software [48] for NCI analysis. Gradient isosurface plots of RDG versus the $\lambda_2 \times \rho(r)$ were viewed by the VMD program [60] based on the outputs of Multiwfn software.

4. Results and discussion

4.1. Experimental results

4.1.1. Spectroscopic characterization of ILs

The FT-IR and ^{1}H NMR spectra of the synthesized ILs were given as supplementary information in Figs. S1 and S2, respectively.

Selected data for [Bn-DBU][CH_3CO_2]. Pale yellow oil; ^{1}H NMR (D_2O, 400.13 MHz) δ (ppm) 7.35 (2H, t, *J* 7.8 Hz, Ar−H), 7.29 (1H, t, *J* 7.0 Hz, Ar−H), 7.17 (2H, d, *J* 7.2 Hz, Ar−H), 4.50 (2H, br s, Ar-CH_2), 3.55 (2H, br s, CH_2), 3.47−3.39 (4H, m, CH_2), 2.71−2.69 (2H, m, CH_2), 2.01−1.99 (2H, m, CH_2), 1.87 (3H, br s, CH_2), 1.60 (4H, br s, CH_2), 1.44 (2H, br s, CH_2); FT-IR (KBr, cm^{-1}): 2935, 2861, 1645, 1620, 1527, 1496, 1325.

Selected data for [Bn-DBU][$PhSO_2$]. Colorless oil; ^{1}H NMR (D_2O, 400.13 MHz) δ (ppm) 7.46 (2H, br s, Ar-CH_2), 7.33−7.21 (6H, m, Ar-CH_2), 7.06 (2H, d, *J* 6.4 Hz Ar-CH_2), 4.51 (2H, br s, Ar-CH_2), 3.40 (2H, br s, CH_2), 3.30 (2H, br s, CH_2), 3.23 (2H, br s, CH_2), 2.53 (2H, br s, CH_2), 1.89−1.84 (2H, m, CH_2), 1.47 (4H, br s, CH_2), 1.28 (2H, br s, CH_2); FT-IR (KBr, cm^{-1}): 2932, 2864, 1645, 1620, 1527, 1448, 1274, 1025.

Selected data for [Bn-DBU][HCO_3]. Pale yellow oil; ^{1}HNMR (D_2O, 400.13 MHz) δ (ppm) 7.33−7.27 (3H, m, Ar−H), 7.16 (2H, d, *J* 6.4 Hz, Ar−H), 4.49 (2H, br s, Ar-CH_2), 3.53 (2H, br s, CH_2), 3.44 (2H, br s, CH_2), 3.39 (2H, br s, CH_2), 2.69 (2H, br s, CH_2), 1.98 (4H, br s, CH_2), 1.58 (2H, br s, CH_2), 1.42 (2H, br s, CH_2); FT-IR (KBr, cm^{-1}): 3422, 3106, 3030, 2934, 2862, 1645, 1620, 1526, 1450, 1326.

Selected data for [Bn-DBU][CF_3CO_2]. Pale Yellow oil; ^{1}HNMR (D_2O, 500 MHz) δ (ppm) 7.45 (2H, t, *J* 7.3 Hz, Ar−H), 7.39 (1H, t, *J* 7.1 Hz, Ar−H), 7.27 (2H, d, *J* 7.4 Hz, Ar−H), 4.45 (2H, br s, Ar-CH_2), 3.57−3.48 (6H, m, CH_2), 2.82−2.80 (2H, m, CH_2), 2.11−2.08 (2H, m, CH_2), 1.70 (4H, br s, CH_2), 1.53 (2H, br s, CH_2); FT-IR (KBr, cm^{-1}): 3126, 3058, 2936, 1710, 1647, 1598, 1447, 1205, 1122.

Selected data for [Bn-DBU][BF_4]. Colorless oil; ^{1}HNMR (D_2O, 400.13 MHz) δ (ppm) 7.32 (2H, t, *J* 6.4 Hz, Ar−H), 7.27 (1H, t, *J* 6.4 Hz, Ar−H), 7.15 (2H, d, *J* 6.4 Hz, Ar−H), 4.49 (2H, br s, Ar-CH_2), 3.52 (2H, br s, CH_2), 3.43 (2H, br s, CH_2), 3.38 (2H, br s, CH_2), 2.69 (2H, br s, CH_2), 1.97 (2H, br s, CH_2), 1.57 (4H, br s, CH_2), 1.42 (2H, br s, CH_2); FT-IR (KBr, cm^{-1}): 3098, 3030, 2934, 2864, 1645, 1620, 1526, 1054, 1451, 1326, 1054.

Selected data for [Bn-DBU][SCN]. Pale Yellow oil; ^{1}HNMR (D_2O, 400.13 MHz) δ (ppm) 7.38−7.28 (3H, m, Ar−H), 7.17 (2H, d, *J* 6.4 Hz, Ar−H), 4.50 (2H, br s, Ar-CH_2), 3.54 (2H, br s, CH_2), 3.45 (2H, br s, CH_2), 3.41 (2H, br s, CH_2), 2.71 (2H, br s, CH_2), 1.99 (2H, br s, CH_2), 1.59 (4H, br s, CH_2), 1.44 (2H, br s, CH_2); FT-IR (KBr, cm^{-1}): 3120, 2934, 2863, 2056, 1645, 1620, 1526, 1450, 1324, 742.

4.1.2. Thermogravimetric analysis

Thermal stability is an important property of ILs that largely depends on their salt structure, i.e., the type of the paired cation and anion. Fig. 4 exhibits the DSC and TGA curves of the ILs synthesized by the herein presented method. As this Fig. shows, the decomposition temperatures (T_d) of the synthesized ILs fall within the rage of 160−300 °C. The first step of weight-loss up to the main degradation step in the TGA curves of these ILs can be attributed to the evaporation of the water sorbed by the samples upon exposure to moist air. The first step of weight-loss for [X][SCN], [X][BF_4] and [X][HCO_3] ILs (X = [Bn−DBU]) occurs at wider temperature range, indicating that weight-loss in these ILs is greater than other synthesized ILs. Noticeably, this step is composed of two smaller steps in the case of [X][SCN]. These facts can be better interpreted as the anions in these ILs undergo splitting during the initial step to more stable anions and the relevant salts. The initial weight-loss step corresponds to an endothermic trace in the DSC curves of the ILs peaking at around 90−94 °C is attributed to the evaporation of the water molecules sorbed by the samples previously. The separate experiments confirmed the hygroscopic nature of the ILs; the Karl-Fischer measurement proved that [X][CF_3CO_2] sorbed about 11% water from a moist air within 10 h. The main disintegration step of the ILs starts at the onset points (T_d) of 160, 180, 220, 230, 270, and 300 °C for [X][CH_3CO_2], [X][CF_3CO_2], [X][$PhSO_2$], [X][HCO_3], [X][BF_4], and [X][SCN] ILs, respectively, displaying a large dependence to the nature of the constituting anions. Certainly, many factors including H-bonding, non-bonding (van der Waals) attractions, proximity and the strength of ionic bonds between the counter ions affect the thermal stability of the ILs. The nature of anion would keenly affect the orientation and position of H-bonds as well as the proximity to the cation (Bn−DBU). As can be seen, the ILs composed of weakly coordinating (less basic) anions are more stable than the others [61–65]. For example, $CF_3CO_2^-$ anion is a weaker base than $CH_3CO_2^-$ that leads to the greater thermal stability of [X][CH_3CO_2] IL. Likewise, the order of thermal stability for the other ILs was found to be as [X][$PhSO_2$] < [X][HCO_3] < [X][BF_4] < [X][SCN], which corresponds with the decreasing order for basicity of their anions. The DSC trace of [X][CF_3CO_2] displays two additional endotherms after the onset point of the main weight-loss step, peaking at around 204

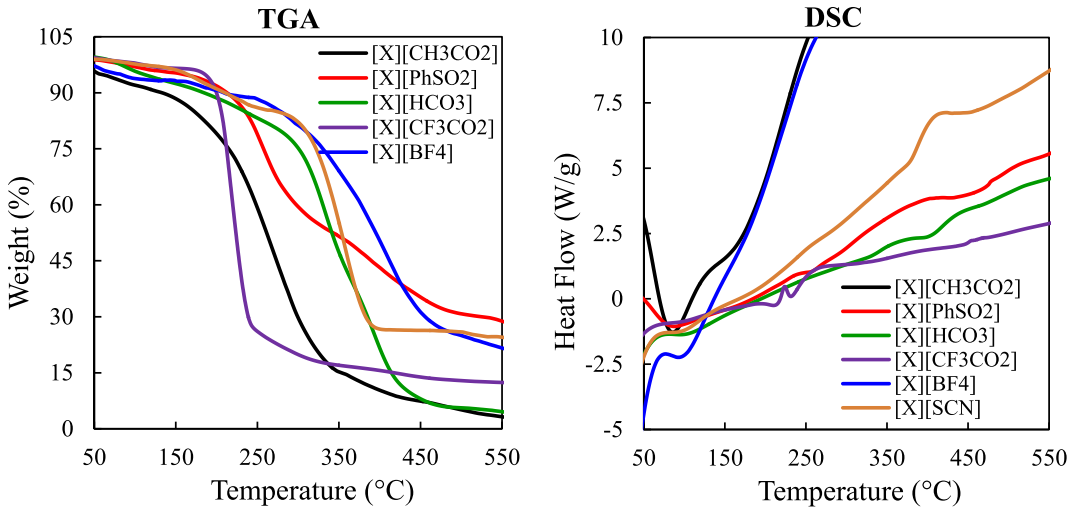

Fig. 4. TGA–DSC curves for [Bn–DBU][CH_3CO_2], [Bn–DBU][$PhSO_2$], [Bn–DBU][HCO_3], [Bn–DBU][CF_3CO_2], [Bn–DBU][BF_4] and [Bn–DBU][SCN] ILs.

and 236 °C. The similar weak endotherms can be detected in the DSC curves of the other ILs.

4.2. Theoretical results

4.2.1. MESP maps and most stable configurations

Molecular electrostatic potential surface (MESP) is a real physical observable property that can be determined by experimentally as well as computationally methods. The electrostatic potential $V(\mathbf{r})$ is a local property, which has a specific value at each point **r** in the space of the system. Since MESP is related to electron density, it is a very useful descriptor in understanding electrophilic and nucleophilic attacks in chemical reactions. It can be used to recognize regions of local negative and positive potential in a molecule and to explain the intermolecular interactions between polar species. Thus, inspection of MESP can be used to understand non-covalent intramolecular interactions. To make the electrostatic potential energy data easy to interpret, a color spectrum is employed to convey the varying intensities of the electrostatic potential energy values. Red color represents regions of most negative electrostatic potential with the lowest electrostatic potential energy value that act as an electrophilic attack, blue represents regions of most positive electrostatic potential with highest EP energy value which act as a nucleophile attack, and green represents region of zero potential [48,66–68].

There are the several possible interaction sites around $[Bn–DBU]^+$ cation that anions can be approached. To understand the behavior of interaction between the cation and the anions in the DBU based ILs, electrostatic potential surfaces (ESP) maps of anions and cation in [Bn–DBU][$Y_{1\text{-}8}$] ($Y_{1\text{-}8} = CH_3CO_2^-$, $PhSO_2^-$, $PhSO_3^-$, HCO_3^-, HSO_4^-, $CF_3CO_2^-$, BF_4^- and SCN^-) ion pairs were calculated at M06-2X/6–311++G(d,p) level of theory. The EPS maps of the free cation and anions are assessed in Fig. 5 where the blue-colored surfaces represent the positive electrostatic potential and the red-colored surfaces signify the negative one. Electrostatic potential surface maps for the anions and the cation reveal well sites in which are most electron-rich and most electron-poor. As can be observed in this Fig., all regions around the $[Bn–DBU]^+$ cation have positive electrostatic potential. Because of darker blue-colored surface, the positive charge distributions were mostly located on N1 (surface map value = 0.1402), N8 (surface map value = 0.1267), C7 (surface map value = 0.1321) and C–H bonds of the cation. A negative charge concentration were seen over the oxygen, fluorine and nitrogen atoms of $CH_3CO_2^-$, $PhSO_2^-$, $PhSO_3^-$, HCO_3^-, HSO_4^-, $CF_3CO_2^-$, BF_4^- and SCN^- anions, respectively, as indicated by the red color.

According to ESP maps, the main interactions occur between the oxygen, fluorine and nitrogen atoms of $CH_3CO_2^-$, $PhSO_2^-$, $PhSO_3^-$, HCO_3^-, HSO_4^-, $CF_3CO_2^-$, BF_4^- and SCN^- anions and positive regions(N1–C7–N8 and C–H) of $[Bn–DBU]^+$ cation. Accordingly, hydrogen bond is formed between the oxygen, fluorine, sulfur and nitrogen atoms of $CH_3CO_2^-$, $PhSO_2^-$, $PhSO_3^-$, HCO_3^-, HSO_4^-, $CF_3CO_2^-$, BF_4^- and SCN^-anions and C–H bonds of the [Bn-DBU]$^+$ cation.

The value of MESP minimum (V_{min}) is a sensitive descriptor that shows the shift of electron density from one atom to another in a non-covalent binding interaction. The V_{min} value of heteroatoms of $CH_3CO_2^-$, $PhSO_2^-$, $PhSO_3^-$, HCO_3^-, HSO_4^-, $CF_3CO_2^-$, BF_4^- and SCN^- anions involved in interactions with cation is −157.3, −142.7, −129.7, −149.8, −130.0, −138.4, −131.9, −124.8 kcal mol^{-1}, respectively. V_{min} in the MESP topography located at the lone pair region provides a quantitative interpretation of the strength and position of the lone pair. Magnitude of the V_{min} value represents a more localized and electron dense lone pair. Thus, it is predicted that strength of interaction to be different in ion pairs formed by various anions.

The most stable configurations obtained for the ILs from interaction between various anions and $[Bn–DBU]^+$ cation are represented in Fig. 6. This Fig. shows that [Y_2] and [Y_6] anions locate above and parallel to the seven membered ring in [Bn–DBU][$PhSO_2$] and [Bn–DBU][CF_3CO_2] ILs, while other anions ([Y_1], [$Y_{3\text{-}5}$] and [$Y_{7\text{-}8}$]) localize above and nearly perpendicular to this ring. It should be noted that the [Bn–DBU][SCN] IL adopts the two configurations so that structure (b) is more stable than (a). So, nine structures, namely [X][$Y_{1–8}$], (X = $[Bn–DBU]^+$ and $Y_{1\text{-}8} = [CH_3CO_2]^-$, $[PhSO_2]^-$, $[PhSO_3]^-$, $[HCO_3]^-$, $[HSO_4]^-$, $[CF_3CO_2]^-$, $[BF_4]^-$, $[SCN]^-$(a) and $[SCN]^-$(b)) ILs were predicted.

Fig. 7 shows the calculated ESP maps of the ILs. As can be seen, charge distributions occur between $[Bn–DBU]^+$ cation and anions in [Bn–DBU][$Y_{1–8}$] ILs. The color codes of these maps for the ILs were in the range of −0.076 to 0.076 au for [Bn–DBU][Y_1] IL, −0.072 to 0.072 au for [Bn–DBU][Y_2], −0.072 to 0.072 au for [Bn–DBU][Y_3], −0.091 to 0.091 au for [Bn–DBU][Y_4], −0.075 to 0.075 au for [Bn–DBU][Y_5], −0.074 to 0.074 au for [Bn–DBU][Y_6], −0.081 to 0.081 au for [Bn–DBU][Y_7], −0.096 to 0.096 au for [Bn–DBU][Y_8] (a) and −0.076 to 0.076 au for [Bn–DBU][Y_8] (b) ILs, respectively.

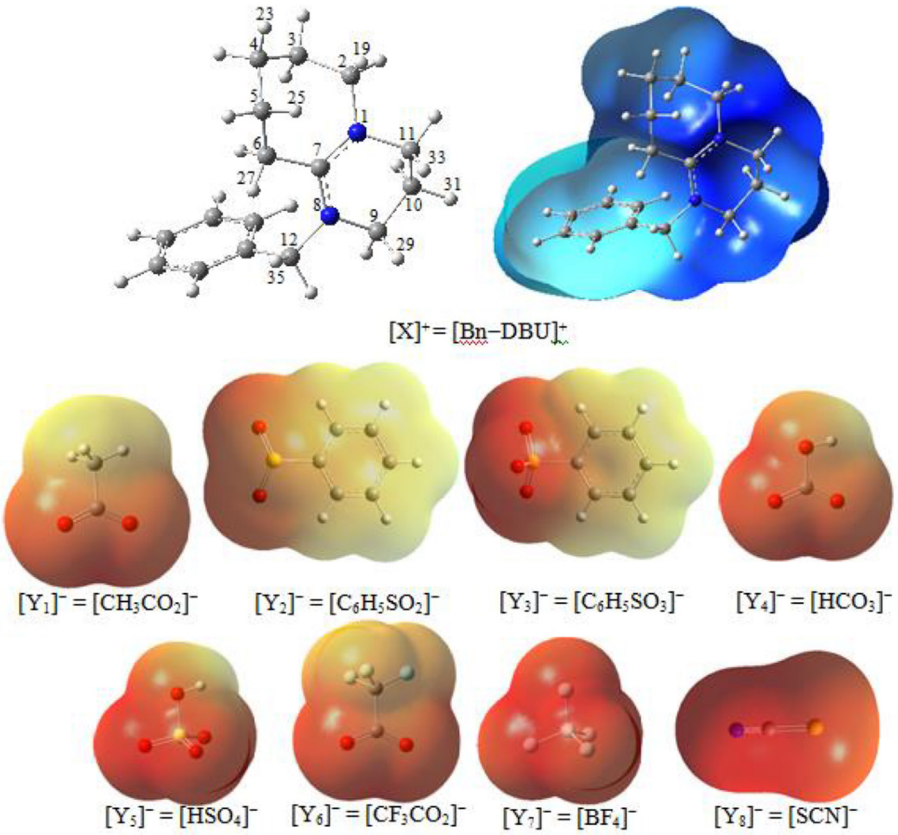

Fig. 5. Structures and calculated ESP maps of the isolated $[Bn-DBU]^+$ cation and $CH_3CO_2^-$, $C_6H_5SO_2^-$, $C_6H_5SO_3^-$, HCO_3^-, HSO_4^-, $CF_3CO_2^-$, BF_4^- and SCN^- anionsat the M06-2X/6311++G(d,p) level of theory (isovalue: 0.0004). The N, C, O, S, F and H atoms in all structures are shown as blue, gray, red, yellow, bluish and white colors.

4.2.2. Interaction energies

The electronic interaction energies, enthalpies and Gibbs free energies for ion pair formation of [Bn-DBU][Y_{1-8}], (Y_{1-8} = $[CH_3CO_2]^-$, $[PhSO_2]^-$, $[PhSO_3]^-$, $[HCO_3]^-$, $[HSO_4]^-$, $[CF_3CO_2]^-$, $[BF_4]^-$ and$[SCN]^-$) ILs in the gas phase are reported in Table 1. As can be observed, the range of BSSE and ZPVE corrected interaction energies (ΔE_c) is from −87.75 kcal mol^{-1} to −100.69 kcal mol^{-1} in [Bn-DBU][Y_{1-8}] ILs at M06−2X/6−311++G(d,p) level of theory. Also, ΔH and ΔG values with the BSSE and ZPVE corrections for [Bn-DBU][Y_{1-8}] ILs are in the range of −85.96 to −97.71 kcal mol^{-1} and −73.24 to −85.21 kcal mol^{-1}, respectively. The results show that the interaction between cation and anion in the gas phase is very strong and the strongest interaction is more sensible for the [Bn-DBU][CH_3CO_2] IL with ΔG of −85.21 kcal mol^{-1}. The second most stable IL is the [Bn-DBU][$PhSO_2$] one with ΔG value of −84.00 kcal mol^{-1}. Based on the BSSE and ZPVE corrected ΔG, the estimated stability order of the ILs formed from interaction between $[Bn-DBU]^+$ cation and the anions is [Bn-DBU][CH_3CO_2] > [Bn-DBU][$PhSO_2$] > [Bn-DBU][HCO_3] > [Bn-DBU][$PhSO_3$] > [Bn-DBU][HSO_4] > [Bn- [Bn-DBU][SCN] (b) > DBU][CF_3CO_2] > [Bn-DBU][SCN] (a) > [Bn-DBU][BF_4]. It is clear that the most and least stable structures correspond to ILs formed of the interaction of $[Bn-DBU]^+$ cation with $[CH_3CO_2]^-$ and $[BF_4]^-$anions, respectively.

Because the interactions between $[Bn-DBU]^+$ cation and the anions in the ILs are influenced by van der Waals interactions, the interaction energies calculated by M06-2X functional can be changed by the inclusion of empirical dispersion. Accordingly, effects of dispersion correction on the interaction energy of studied ILs were explored by M06-2X-GD3 dispersion corrected functional. The dispersion-corrected interaction energies are given in Table 1. As can be seen in Table 1, interaction energies calculated by dispersion-corrected M06-2X-GD3 hybrid functional is greater than M06-2X one. The interaction energy values corrected with dispersion (ΔE_{disp}) for $[Bn-DBU]^+$[Y_{1-8}], (Y_{1-8} = $[CH_3CO_2]^-$, $[PhSO_2]^-$, $[PhSO_3]^-$, $[HCO_3]^-$, $[HSO_4]^-$, $[CF_3CO_2]^-$, $[BF_4]^-$,$[SCN]^-$(a) and $[SCN]^-$(b)) ILs at M06−2X-GD3/6−311++G(d,p) level of theory are −102.56, −104.34, −100.29, −99.11, −97.87, −94.05, −92.06, −89.38 and −89.17 kcal mol^{-1}, respectively. As can be seen in Table 1, ΔE_{disp} values of the ILs increases on going from M06-2X to M06-2X-GD3. Comparison of the interaction energies calculated by M06-2X and M06-2X-GD3 functionals reveals that the range of the dispersion contribution varies from 2.51% for [Bn-DBU][HCO_3] to 3.50% for [Bn-DBU][$PhSO_2$]. Percentage of its contribution to the interaction energies is 2.54, 3.50, 3.40, 2.51, 2.76, 3.01, 2.77, 2.57, 2.59% for [Bn−DBU][Y_{1-8}], (Y_{1-8} = $[CH_3CO_2]^-$, $[PhSO_2]^-$, $[PhSO_3]^-$, $[HCO_3]^-$, $[HSO_4]^-$, $[CF_3CO_2]^-$, $[BF_4]^-$,$[SCN]^-$(a) and $[SCN]^-$(b)) ILs, respectively.

The dispersion corrected interaction energies obtained by using M06-2X-D3 functional for [Bn-DBU][$PhSO_2$], [Bn-DBU][$PhSO_3$],[Bn-DBU][CF_3CO_2]ILs are more than other ionic liquids. The consequence of ΔE_{disp} calculated by using M06-2X-GD3 functional is [Bn-DBU][$PhSO_2$] > [Bn-DBU][CH_3CO_2] > [Bn-DBU][$PhSO_3$] > [Bn-DBU][HCO_3] > [Bn-DBU][HSO_4] > [Bn-DBU][CF_3CO_2] > [Bn-DBU][BF_4] > [Bn-DBU][SCN] (a) > [Bn-DBU][SCN] (b). This trend can be explained by charge transferred from anion to cation in which is greater for anions with stronger basicity property.

The nature of interaction between the cation and the anions can be specified by the energy decomposition analysis (EDA) method.

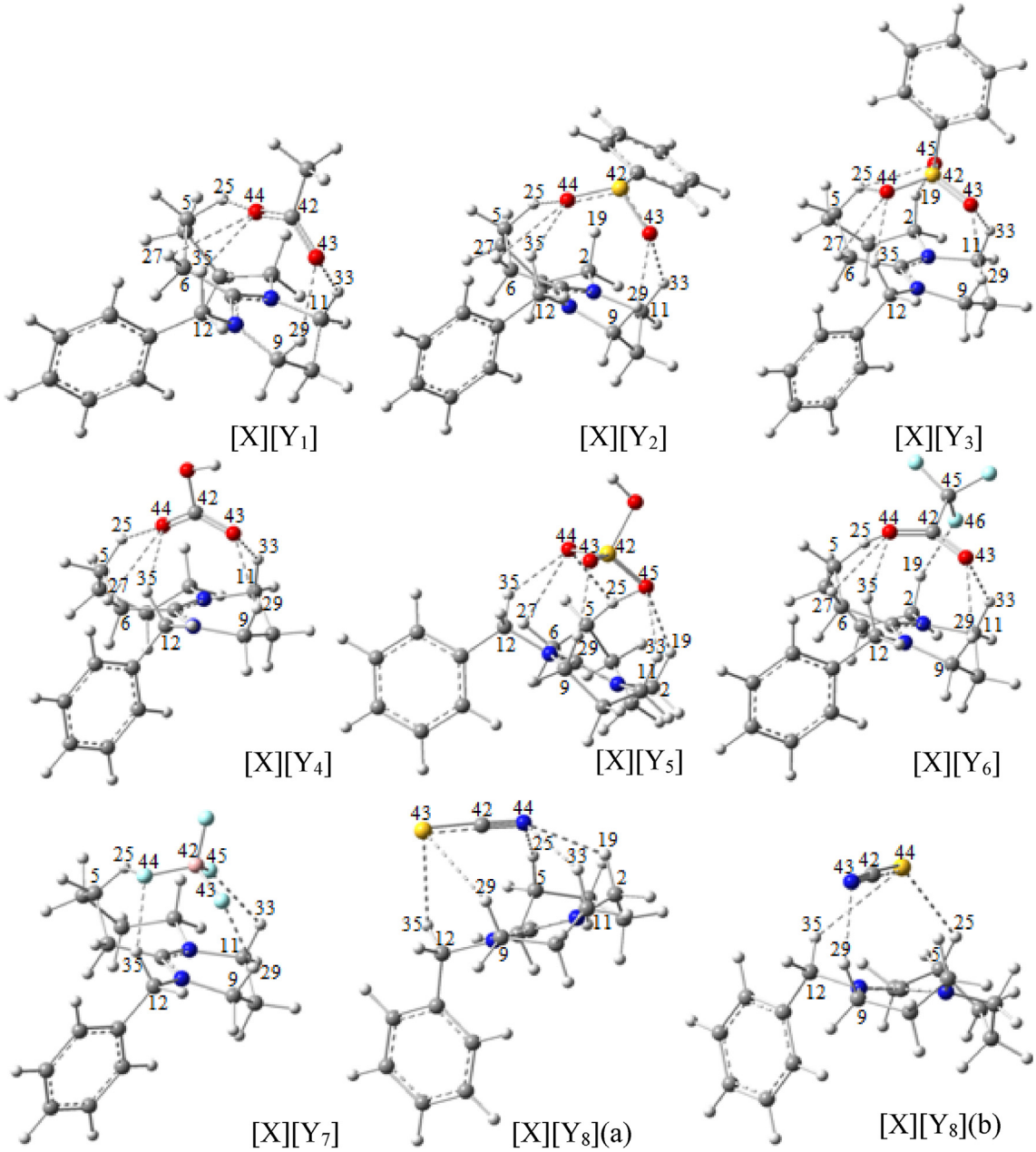

Fig. 6. The optimized [X][Y_{1-8}], (X = [Bn−DBU]$^+$, Y_{1-8} = $CH_3CO_2^-$, $C_6H_5SO_2^-$, $C_6H_5SO_3^-$, HCO_3^-, HSO_4^-, $CF_3CO_2^-$, BF_4^- and [SCN]$^-$ (a, b)) ILs at M06−2X/6−311++G(d,p)level of theory in gas phase.

In EDA, the interaction energy between the two fragments (ΔE_{int}) can be broken into four physically meaningful components: $\Delta E_{int} = \Delta E_{Pauli} + \Delta E_{elect} + \Delta E_{orb} + \Delta E_{disp}$. ΔE_{Pauli} is the repulsive four-electron interactions between occupied orbitals. ΔE_{elect} is the electrostatic interaction energy between the fragments. The orbital interaction, ΔE_{orb}, accounts for charge transfer and polarization contributions. In addition, ΔE_{disp} is the dispersion contribution to interaction energy. The EDA was carried out at the PB86-D3/TZP level of theory. Table 2 lists the results of the EDA calculations at the PB86-D3/TZP level of theory for the ILs. As seen from Table 2, the contribution of the ΔE_{elect} component in each ILs is more than that of the ΔE_{disp} and ΔE_{orb} components ($\Delta E_{elect} > \Delta E_{orb} > \Delta E_{disp}$). It is worth mentioning that the percentage of contribution of the ΔE_{disp} component in the ILs containing $[PhSO_2]^-$, $[PhSO_3]^-$, $[HSO_4]^-$ and $[CF_3CO_2]^-$anions is greater than others. Table 2 also indicates that the electrostatic interaction (ΔE_{elect}) and orbital interaction (ΔE_{orb}) energies have considerable contribution to the binding energy.

4.3. Structural parameters

In this section, we focus on the structural parameters of the most stable configurations of the [Bn-DBU][Y_{1-8}], (Y_{1-8} = $[CH_3CO_2]^-$, $[PhSO_2]^-$, $[PhSO_3]^-$, $[HCO_3]^-$, $[HSO_4]^-$, $[CF_3CO_2]^-$, $[BF_4]^-$ and$[SCN]^-$) ILs, as shown in Fig. 6. It is estimated that the H-bonding can be formed between O, F, N and S atoms of $[Y_{1-8}]^-$ anions and C−H bonds of DBU rings as well as CH_2 group of benzyl group of the [Bn−DBU]$^+$ cation. The nature of anions and their possible arrangements around the cation have many effects on the structure of ion pairs in ILs. In [Bn−DBU][$Y_{1,3-5,7}$] ion pairs, anions lie above the DBU rings and interact with the C−H groups of the

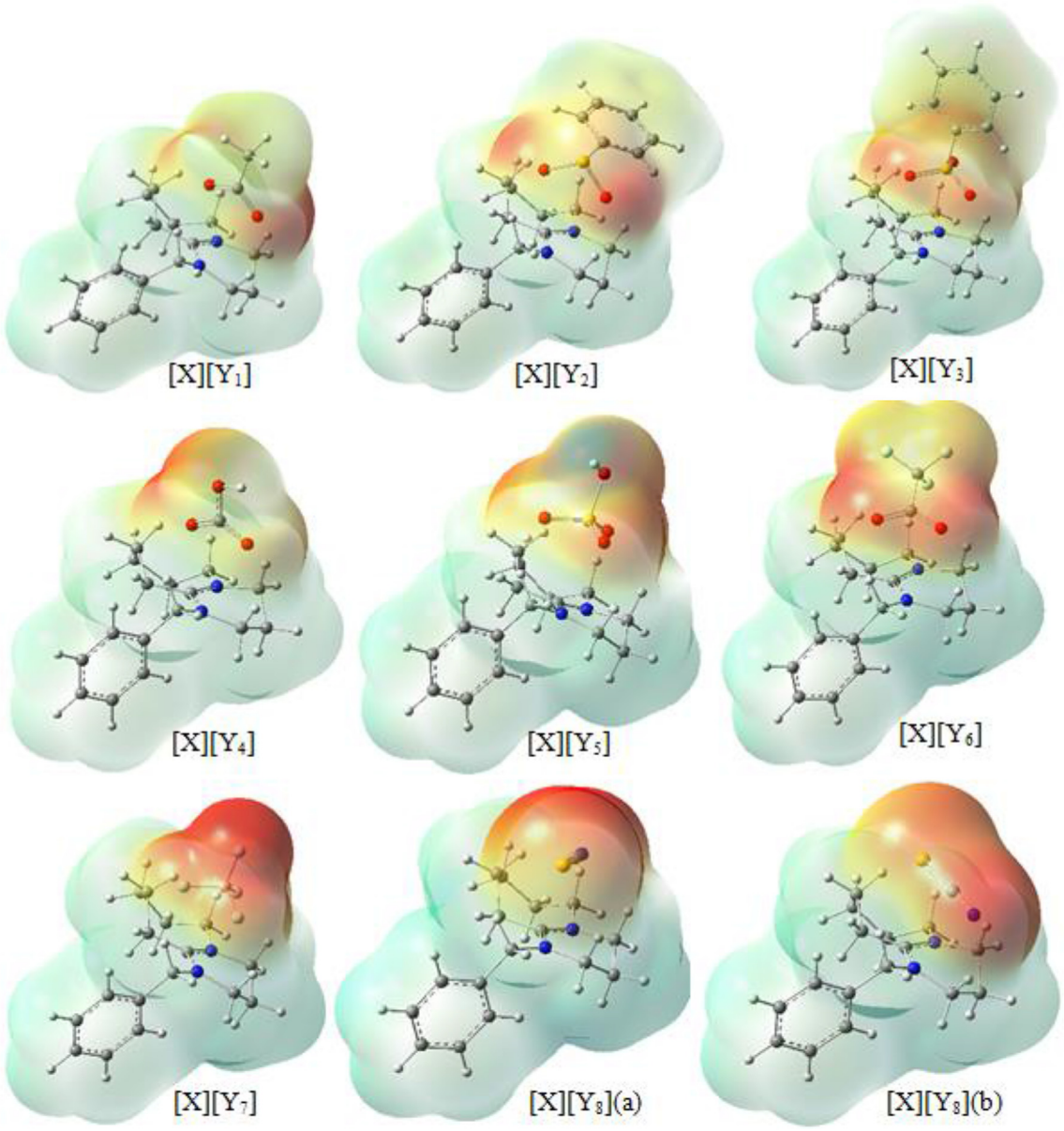

Fig. 7. Electrostatic potentials calculated at the M06-2X/6311++G(d,p) level of theory and mapped on to the 0.0004 electron density isosurface for [X][Y_{1-8}], (X = [Bn−DBU]$^+$, Y_{1-8} = $CH_3CO_2^-$, $C_6H_5SO_2^-$, $C_6H_5SO_3^-$, HCO_3^-, HSO_4^-, $CF_3CO_2^-$, BF_4^- and $[SCN]^-$ (a, b)) ILs.

Table 1
Interaction energies, enthalpies, Gibbs free energies (ΔE, ΔH and ΔG, in kcal mol^{-1}) dipole moments (q, in Debye) in gas phase calculated for [X][Y_{1-8}], (X = [Bn−DBU]$^+$ and Y_{1-8} = $CH_3CO_2^-$, $C_6H_5SO_2^-$, $C_6H_5SO_3^-$, HCO_3^-, HSO_4^-, $CF_3CO_2^-$, BF_4^- and SCN^-(a and b)) ILs at M06−2X/6311++G(d, p) level of theory.

ILs	ΔZPVE	BSSE	ΔE[a]	ΔE_{disp}	ΔE_c	ΔH_c	ΔG_c	q
[Bn-DBU][Y_1]	1.64	1.44	−100.02	−100.78	−96.94	−95.14	−82.67	7.02
[Bn-DBU][Y_2]	1.54	3.36	−100.81	−102.36	−95.90	−94.18	−80.46	7.24
[Bn-DBU][Y_3]	1.54	3.23	−96.99	−98.26	−92.22	−90.85	−76.50	6.72
[Bn-DBU][Y_4]	1.28	1.50	−96.68	−97.34	−93.90	−92.37	−80.74	8.00
[Bn-DBU][Y_5]	1.82	3.43	−95.24	−96.09	−89.98	−88.19	−74.21	8.05
[Bn-DBU][Y_6]	1.46	2.05	−91.30	−92.25	−87.79	−86.16	−72.48	9.90
[Bn−DBU][Y_7]	1.72	2.47	−89.58	−90.29	−85.39	−83.49	−70.76	10.94
[Bn-DBU][Y_8](a)	1.15	1.16	−87.14	−87.61	−84.83	−84.14	−72.26	10.69
[Bn-DBU][Y_8](b)	0.99	1.03	−86.92	−87.40	−84.90	−83.79	−73.30	11.06

a: $\Delta X = X_{elec(IL)} - (X_{elec\ (cation)} + X_{elec\ (anion)})$, X = E, H and G.
b: $\Delta X_c = \Delta X + \Delta ZPEV + BSSE$.

Table 2
Energy Decomposition Analysis (EDA, in kcal mol^{-1}) for [X][Y_{1-8}], (X = [Bn−DBU]$^+$ and Y_{1-8} = $CH_3CO_2^-$, $C_6H_5SO_2^-$, $C_6H_5SO_3^-$, HCO_3^-, HSO_4^-, $CF_3CO_2^-$, BF_4^- and SCN^-(a and b)) ILs at the PBE-D3/TZP Level of Theory.

ILs	ΔE_{Pauli}	ΔE_{elect}	ΔE_{orb}	ΔE_{disp}	ΔE_{int}[a]
[Bn-DBU][Y_1]	36.39	−102.77	−26.46	−9.64	−102.48
[Bn-DBU][Y_2]	41.52	−100.07	−25.92	−18.45	−102.92
[Bn-DBU][Y_3]	32.93	−94.93	−19.94	−15.04	−96.98
[Bn-DBU][Y_4]	33.28	−99.5	−23.78	−9.52	−99.52
[Bn-DBU][Y_5]	32.44	−96.00	−18.38	−14.49	−96.43
[Bn-DBU][Y_6]	31.15	−92.17	−18.26	−12.79	−92.08
[Bn-DBU][Y_7]	29.39	−90.7	−16.3	−10.85	−88.47
[Bn-DBU][Y_8](a)	27.25	−89.69	−16.91	−9.96	−89.31
[Bn-DBU][Y_8](b)	27.47	−88.49	−17.22	−10.52	−88.76

[a] ΔE_{int} Values calculated by ADF are without basis set superposition errors.

cation through heteroatoms. The optimized structure of [Bn−DBU][$PhSO_2$] shows that the [$PhSO_2$]$^-$ anion locates above and parallel to the DBU ring where it can interact simultaneously with the C−H groups of the cation through O atoms and the phenyl aromatic ring. Because of presence of CF_3 group, the structure of [Bn−DBU][CF_3CO_2] IL is different. In this IL, anion interacts with cation through the F and O atoms. It should be noted that the [Bn−DBU][SCN] IL adopts two configurations so that [Bn−DBU][Y_8] (b) structure is slightly more stable than [Bn−DBU][Y_8] (a). Direction of C═S group in two structures is different. The C═S group is directed toward the seven membered ring in structure (b), and in structure (a) locates between six membered ring and CH_2 of benzyl group. The main structural parameters of the ILs calculated at M06−2X/6−311++G(d,p) level of theory are given in Table S1 of supplementary data and Table 3.

Length of the N8−C12 bond between benzyl group and DBU ring in Bn-DBU cation is 1.474 Å that decreases to 1.464, 1.463, 1.466, 1.464, 1.467, 1.496, 1.469, 1.469 (1.467) Å in [Bn−DBU][$Y_{1-8a(b)}$] ILs, respectively, indicating that its value for most stable ILs is lower than less stable ones. It is predicted that this bond is decomposed when IL to be heated. There is a good correlation between N8−C12 bond length and interaction energy as shown in Fig. 8. The N1C7N8 angle of DBU rings in cation is 120.0° that changes to 119.7, 120.6, 120.4, 119.6, 120.6, 120.3, 120.9, 121.4 and 119.1° in [Bn−DBU][Y_8] ILs, respectively.

The C9−H29,C11−H33,C2−H19, C5−H25 and C6−H27 bonds of DBU rings and the C12−H35 bond of the CH_2 group of the benzyl in the cation are generally involved in interaction with O, F, N and S atoms of the [Y_{1-8}]$^-$anions. The average value of C−H bond lengths

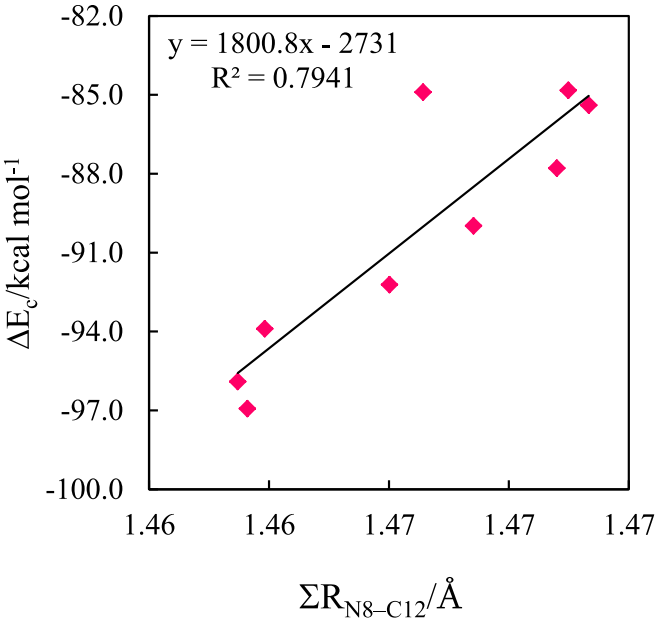

Fig. 8. Correlations between N8−C12bond length and interaction energy for [X][Y_{1-8}], (X = [Bn−DBU]$^+$, Y_{1-8} = $CH_3CO_2^-$, $C_6H_5SO_2^-$, $C_6H_5SO_3^-$, HCO_3^-, HSO_4^-, $CF_3CO_2^-$, BF_4^- and $[SCN]^-$ (a, b)) ILs.

involved in interaction (<C−H>) for [Bn-DBU][Y_{1-8}], (Y_{1-8} = $[CH_3CO_2]^-$, $[PhSO_2]^-$, $[PhSO_3]^-$, $[HCO_3]^-$, $[HSO_4]^-$, $[CF_3CO_2]^-$, $[BF_4]^-$ and$[SCN]^-$ (a,b)) ILs is 1.0920, 1.0901, 1.0912, 1.0911, 1.0913, 1.0907, 1.0916, 1.0936 and 1.0923 Å, respectively. As can be seen in Table 3, increase in the C12−H35 bond length of the CH_2 group of benzyl upon complex formation is 0.0020, 0.0006, 0.0016, 0.0001, 0.0009 and 0.0026 Å in [Bn−DBU][$Y_{1-4,6,8(b)}$], respectively.

The average value of H-bonding distances in [Bn-DBU][Y_{1-8}], Y_{1-8} = $[CH_3CO_2]^-$, $[PhSO_2]^-$, $[PhSO_3]^-$, $[HCO_3]^-$, $[HSO_4]^-$, $[CF_3CO_2]^-$, $[BF_4]^-$ and $[SCN]^-$ (a, b)) ILs is 2.36, 2.32, 2.40, 2.38, 2.42, 2.38, 2.28, 2.65 and 2.66 Å, respectively. As can be seen, with the exception of ILs having $CF_3CO_2^-$ and BF_4^- anions, a good correlation is found between the average value of the H-bonding distances (<C−H···>) and interaction energies. As shown in Fig. 5, anions in ion pairs are located above the DBU rings so that the H-bond angles deviates from the typical H-bond angle. The average value of H-bonding angles (<∠C−H···>) in [Bn-DBU][Y_{1-8}], Y_{1-8} = $[CH_3CO_2]^-$,

Table 3
The selected geometrical parameters having bond lengths and angles for isolated cation and [Bn−DBU][Y_{1-8}], (Y_{1-8} = $CH_3CO_2^-$, $C_6H_5SO_2^-$, $C_6H_5SO_3^-$, HCO_3^-, HSO_4^-, $CF_3CO_2^-$, BF_4^- and SCN^-(a and b)) ILs at M06−2X/6311++G(d, p) level of theory.

	$[X]^+$	[X][Y_1]	[X][Y_2]	[X][Y_3]	[X][Y_4]	[X][Y_5]	[X][Y_6]	[X][Y_7]	[X][Y_8](a)	[X][Y_8](b)
Bond Length/Å										
N8−C12	1.4737	1.4636	1.4635	1.4660	1.4639	1.4674	1.4688	1.4693	1.4690	1.4666
C9−H29	1.0938	1.0922	1.0942	1.0927	1.0918	1.0941	1.0928	1.0927	1.0950	1.0912
C11−H33	1.0945	1.0945	1.0924	1.0938	1.0948	1.0952	1.0920	1.0943	1.0952	1.0948
C2−H19	1.0949	1.0960	1.0943	1.0946	1.0960	1.0954	1.0943	1.0957	1.0958	1.0960
C5−H25	1.0943	1.0909	1.0890	1.0916	1.0913	1.0906	1.0922	1.0907	1.0926	1.0921
C6−H27	1.0891	1.0845	1.0831	1.0831	1.0850	1.0821	1.0847	1.0817	1.0826	1.0872
C12−H35	1.0909	1.0930	1.0916	1.0911	1.0925	1.0904	1.0918	1.0889	1.0897	1.0935
<C−H>	1.0929	1.0920	1.0901	1.0912	1.0911	1.0913	1.0907	1.0916	1.0936	1.0923
<C−H•••>		2.36	2.32	2.40	2.38	2.42	2.38	2.28	2.65	2.66
Angle/°										
∠N1C7N8	120.0	119.7	120.6	120.4	119.6	120.6	120.3	120.9	121.4	119.1
<∠C−H···>		118.7	118.5	126.0	118.7	128.0	121.2	121.3	124.1	129.0
∠C6C7N8C12	0.2	24.0	23.4	12.5	22.7	8.2	12.4	6.0	4.2	17.4
∠C7N8C12C13	68.4	84.4	90.0	80.3	83.6	81.8	76.4	77.7	76.3	78.9
∠N1C7N8C12	176.7	162.8	165.3	170.8	162.3	175.4	167.9	177.8	180.0	164.1
∠N8C12C13C18	28.3	21.6	10.1	19.1	19.9	10.4	27.6	20.1	18.4	23.0

$[PhSO_2]^-$, $[PhSO_3]^-$, $[HCO_3]^-$, $[HSO_4]^-$, $[CF_3CO_2]^-$, $[BF_4]^-$ and $[SCN]^-$ (a, b)) ILs is ranged from 118.5° for [Bn-DBU][Y_2] to 129.0° for [Bn-DBU][Y_8] (b).

The DBU and phenyl rings in the $[Bn\text{-}DBU]^+$ cation are not coplanar. As can be seen, values of ∠C6C7N8C12 and ∠C7N8C12C13 dihedral angles for the ILs increase upon ILs formation and values of ∠N1C7N8C12 and ∠N8C12C13C18 dihedral angles decrease. The increscent of the ∠C6C7N8C12 dihedral angle for the ILs having Y_1 and Y_2 anions is greater than other ILs, which is in good agreement with the greater interaction energies obtained for these ILs.

4.4. Calculated vibrational frequency analysis

The structural changes caused by change in anions are often accompanied by shifts in vibrational frequencies of functional groups involved in interaction. As can be observed in Table S2 of supplementary data, the change in anion leads to alteration of the vibrational frequency of C9—H29, C11—H33, C2—H19, C5—H25and C6—H27 bonds of DBU rings and the C12—H35bond of theCH_2 group of benzyl, in good agreement with the change in their bond lengths. The calculated symmetric vibrational frequencies of CH_2 group of benzyl in [Bn-DBU][$Y_{1,8}$] ILs are 3076.8, 3079.9, 3091.8, 3077.3, 3107.6, 3087.2, 3103.9, 3103.7 and 3081.1 cm^{-1}, respectively. The range of the calculated vibrational frequencies of CH_2 group (3076.8—3107.6 cm^{-1}) is in good agreement with the range of experimental values 2932.4—3120.2 cm^{-1}. Therefore, the calculated structures are close to the real structures in which assigned experimentally. In spite of the absence of the solvation effect, the M06-2X functional produces a good overall agreement with IR measurements.

Also, vibrational frequency of C═O, S═O, B—F and C—N groups of anions involved in interactions were assigned. The calculated high intensity vibrational frequency of interacting C═O group in ILs composed of Y_1, Y_4 and Y_6 is 1666.5, 1752.2 and 1788.5 cm^{-1}, respectively, that are in good agreement with the experimental values 1620.8, 1620.6 and 1647.6 cm^{-1}. For S═O group, the vibrational frequency of a strong peak in ILs having Y_2, Y_3 and Y_5 is 1027, 1190 and 1069.9 cm^{-1}, respectively, that close to the experimental value of 1025.7 cm^{-1}. The calculated and experimental asymmetric vibrational frequency of B—F in Y_7 is 1049 and 1054.8 cm^{-1}, respectively. The experimental vibrational frequency of C≡N is 2056.51 cm^{-1} that is close to the theoretical value 2183.0 cm^{-1}. Despite the solvation effect, the theoretical vibrational frequencies are generally in good agreement with experimental ones. Because of the effect of the solvation on experimental results, the difference between theoretical and experimental results is logical.

4.5. AIM analysis

The quantum theory of atoms in molecules (QTAIM) can be used for characterization of the chemical and non-chemical bonds in the molecules [69,70]. For the studied ILs, values of the electronic density, ρ(r), its corresponding Laplacian, $\nabla^2\rho(r)$, and electronic energy density, H(r) at hydrogen bond critical points (HBCPs) at M06—2X/6—311++G(d,p) level of theory are listed in Table S3 of supplementary data. The molecular graphs including the bond critical points (BCPs) (red spheres), ring critical points (RCPs) (yellow spheres), cage critical points (CCPs) (green spheres) and bond paths for all [Bn—DBU][$Y_{1\text{-}8}$] ILs are shown in Fig. 9. As can be seen, the number of CPs is different in intermolecular regions of the ion pairs.

Fig. 10 displays the correlation between the average values of the electron densities at all HBCPs (<$\rho(r)_H$…>) and interaction energy of [Bn-DBU][Y_{1-8}] ILs. The <ρ(r)> at HBCPs decreases on going from [Y_1] anion to [Y_8] one as the interaction energy decreases. Thus, H-bonding interactions in most stable complexes are stronger than less stable ones. The results of the electron density property in Table S2 shows that the H(r) and $\nabla^2\rho(r)$ at all hydrogen bonds critical points (C—H···) of [X][$Y_{1\text{-}8}$] ILs are positive, indicating that the nature of these H-bonds in all HBCPs of [X][$Y_{1\text{-}8}$] ILs is electrostatic.

4.6. NBO analysis

The strength of interaction between cation and anion in ILs can be analyzed using natural bond orbital calculations [71—73]. The results of NBO including charge transfer energies ($E^{(2)}$), natural charge, charge transfer (CT) and occupancy of NBOs at M06—2X/6—311++G(d,p) level of theory are given in Table 4.

The results of the NBO analysis reveal that the LP(O) → σ*(C—H), LP(F) → σ*(C—H) and LP(Nor S) → σ*(C—H), (C—H = (C9—H29), (C11—H33), (C2—H19), (C5—H25), (C6—H27) and (C12—H35)) donor acceptor interactions are most important intermolecular charge transfer interactions between anions and cation in [BN-DBU][$Y_{1\text{-}8}$] ILs. The NBO data indicate that the sum of charge transfer energies $E^{(2)}$ from anionic unit to cationic one through all interactions ($\sum E^{(2)}$ (A_{unit} → C_{unit})) in [Bn-DBU][Y_{1-8}], $Y_{1\text{-}8} = [CH_3CO_2]^-$, $[PhSO_2]^-$, $[PhSO_3]^-$, $[HCO_3]^-$, $[HSO_4]^-$, $[CF_3CO_2]^-$, $[BF_4]^-$ and $[SCN]^-$ (a, b)) ILs is 32.83, 30.16, 23.42, 30.73, 23.09, 15.49, 27.27, 14.95 and 24.05 kJ mol^{-1}, respectively. It can be seen that the sum of charge transfer energies from anion to cation in the ILs includingY_1, Y_2 and Y_4 anions is more than other ILs, in good agreement with greater interaction energy (ΔE_c) obtained for [X][$Y_{1,2,4}$] ILs.

In conventional hydrogen bonds, positive charge of the H atoms involved in H-bonding increases. The natural charges calculated at M06—2X/6—311++G(d,p) level of theory are given in Table 4. The positive charge of H29, H33, H25 and H35 atoms in C9—H29, C11—H33, C5—H25, C6—H27 and C12—H35 bonds increases upon ILs formation for all ILs, so that this increase for H29, H33 and H25 atoms is more than other H atoms. In addition, the increase in positive charges of hydrogen atoms is higher in[X][$Y_{1\text{-}3,5\text{-}6}$]ILs than other ILs due to the type and position of anions relative to the cation and formation of hydrogen bonds.

The cation moiety of the ILs carries positive charges, but the charge distribution in different parts of cation is not uniform. The positive charges carried by DBU and phenyl rings and CH_2 group of cation, are shown in Table 4. As can be observed, the positive charge is mostly located on the DBU rings of [X][$Y_{1\text{-}8}$] ILs. DBU rings and benzyl group carry the positive charges of 0.706 and 0.293 in the $[BN\text{-}DBU]^+$ cation. These values decrease to (0.656 and 0.263), (0.649 and 0.269), (0.667 and 0.275), (0.666 and 0.266), (0.667 and 0.279), (0.674 and 0.276), (0.684 and 0.283), (0.672 and 0.277) and (0.661 and 0.274)in [X][$Y_{1\text{-}8}$], $Y_{1\text{-}8} = [CH_3CO_2]^-$, $[PhSO_2]^-$, $[PhSO_3]^-$, $[HCO_3]^-$, $[HSO_4]^-$, $[CF_3CO_2]^-$, $[BF_4]^-$ and $[SCN]^-$ (a, b)) ILs, respectively. The trend found for amount of positive charge carried by the DBU rings and benzyl group of the ILs is as follows: [X][Y_7]>[X][Y_6] >[X][Y_8](a)>[X][Y_5] > [X][Y_3] > [X][Y_8](b)> [X][Y_4].[X][Y_1] > [X][Y_2]. This reveals that charge transfer (CT) takes place from anion to cation that leads to decreasing of cation charge. Here, the charge transfer is defined as the difference between sum of atomic charges on complexed and isolated anion. Results of population analysis given in Table 4 indicate that the charge transfer occurs from [$Y_{1\text{-}8}$] anions to cation $[Bn\text{—}DBU]^+$. The CT values obtained for [Bn-DBU][$Y_{1\text{-}8}$], $Y_{1\text{-}8} = [CH_3CO_2]^-$, $[PhSO_2]^-$, $[PhSO_3]^-$, $[HCO_3]^-$, $[HSO_4]^-$, $[CF_3CO_2]^-$, $[BF_4]^-$ and $[SCN]^-$ (a, b)) ILs are 0.0808, 0.0822, 0.0575, 0.0681, 0.0533, 0.0501, 0.0329, 0.0514 and 0.0653, respectively.

Fig. 11 shows the correlation between values of CT values and interaction energies for [X][$Y_{1\text{-}8}$], $Y_{1\text{-}8} = [CH_3CO_2]^-$, $[PhSO_2]^-$, $[PhSO_3]^-$, $[HCO_3]^-$, $[HSO_4]^-$, $[CF_3CO_2]^-$, $[BF_4]^-$ and $[SCN]^-$ (a, b)) ILs.

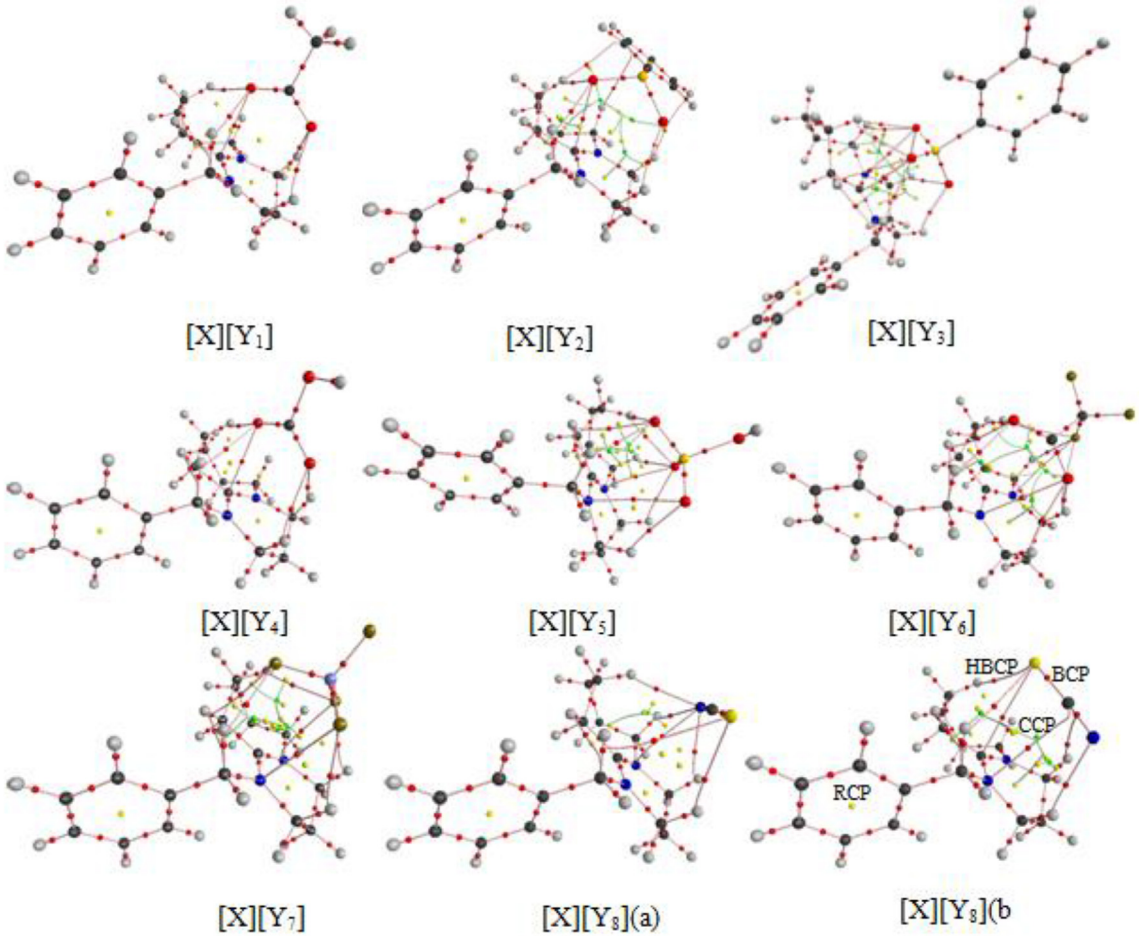

Fig. 9. The molecular graphs contains the bond critical points (BCPs) (red spheres), ring critical points (RCPs) (yellow spheres), cage critical points (CCPs) (green spheres) and bond paths for [X][$Y_{1\text{-}8}$], (X = [Bn−DBU]$^+$, $Y_{1\text{-}8}$ = $CH_3CO_2^-$, $C_6H_5SO_2^-$, $C_6H_5SO_3^-$, HCO_3^-, HSO_4^-, $CF_3CO_2^-$, BF_4^- and $[SCN]^-$ (a, b)) ILs.

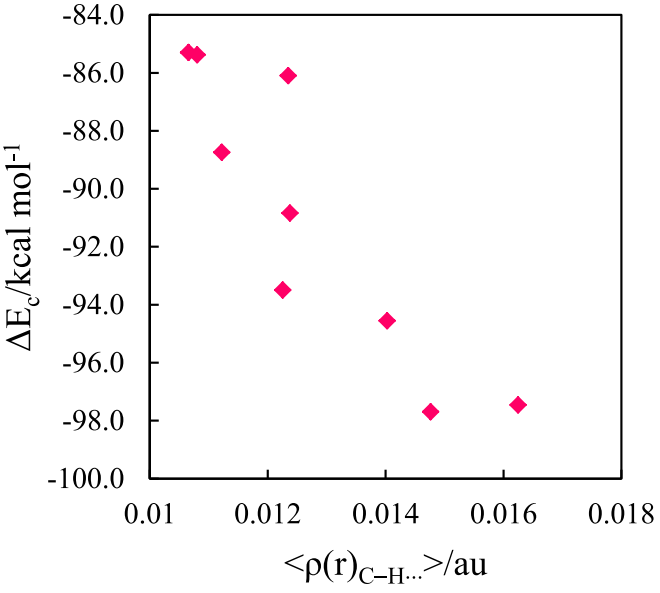

Fig. 10. Correlation between corrected interaction energies and the average of the electron densities at all hydrogen bond critical points (<$\rho(r)_{C\cdots H}$...>) in inter-ionic region of[X][$Y_{1\text{-}8}$], (X = [Bn−DBU]$^+$, $Y_{1\text{-}8}$ = $CH_3CO_2^-$, $C_6H_5SO_2^-$, $C_6H_5SO_3^-$, HCO_3^-, HSO_4^-, $CF_3CO_2^-$, BF_4^- and $[SCN]^-$ (a, b)) ILs.

There is a nearly linear correlation between CT values and interaction energies, with the exception of that found for [Bn-DBU][Y_8] IL. The results show that the CT value for ILs having the [$Y_{1\text{-}2}$] anions is greater than other ones. The CT decreases on going from [Y_1] anion to [Y_8] one as the interaction energy decreases (with the exception of ILs having [Y_8] anion). Fig. 12 shows a relationship between sum of the positive charges carried by DBU rings ($\sum q_{DBU}$) and CT for [X][$Y_{1\text{-}8}$], $Y_{1\text{-}8}$ = $[CH_3CO_2]^-$, $[PhSO_2]^-$, $[PhSO_3]^-$, $[HCO_3]^-$, $[HSO_4]^-$, $[CF_3CO_2]^-$, $[BF_4]^-$ and $[SCN]^-$ (a, b)) ILs. As can be observed, increase in CT value is accompanied by a decrease in positive charge of the DBU rings.

4.7. Non-covalent interaction (NCI) analysis

Based on the electron density and its derivatives, NCI index can be used to detect non-covalent interactions (van der Waals interactions, hydrogen bonds, and steric repulsion) in real space. The second eigen value (λ_2) of the electron-density (second derivative) Hessian matrix, $\nabla^2\rho(r) = \lambda_1 + \lambda_2 + \lambda_3$, ($\lambda_1 < \lambda_2 < \lambda_3$) and electron density ρ are used in this analysis. Based on the type of interaction, the second eigenvalue (λ_2) can be negative, positive or zero. The sign of λ_2 can utilize to distinguish bonded (H-bonding, $\lambda_2 < 0$) from non-bonded (repulsion, $\lambda_2 > 0$) interactions.

The strong steric effect and hydrogen bonding always have $\rho > 0$, while the regions correspond to vdW interactions always have $\rho \approx 0$. While, the sign of λ_2 provides information about the types of weak interactions, the electron density values can be used for

Table 4
NBO data calculated for [X][Y_{1-8}], (X = [Bn−DBU]$^+$ and Y_{1-8} = $CH_3CO_2^-$, $C_6H_5SO_2^-$, $C_6H_5SO_3^-$, HCO_3^-, HSO_4^-, $CF_3CO_2^-$, BF_4^- and SCN^-(a and b)) ILs and isolated cation at M06−2X/6311++G(d, p) level of theory.

	[X]$^+$	[X][Y_1]	[X][Y_2]	[X][Y_3]	[X][Y_4]	[X][Y_5]	[X][Y_6]	[X][Y_7]	[X][Y_8](a)	[X][Y_8](b)
q_{H19}	0.2163	0.2579	0.2597	0.2536	0.2555	0.2573	0.2527	0.2514	0.2510	0.2624
q_{H23}	0.2146	0.2615	0.2581	0.2567	0.2592	0.2487	0.2593	0.2385	0.2434	0.2498
q_{H25}	0.2138	0.2102	0.2305	0.2449	0.2114	0.2333	0.2232	0.2220	0.2410	0.2136
q_{H29}	0.2184	0.2037	0.2051	0.2065	0.2048	0.2074	0.2077	0.2078	0.2093	0.2070
q_{H31}	0.2064	0.2501	0.2481	0.2552	0.2500	0.2489	0.2272	0.2433	0.2544	0.2348
q_{H33}	0.2459	0.2563	0.2534	0.2577	0.2574	0.2558	0.2714	0.2551	0.2425	0.2627
q_{H35}	0.2216	0.2514	0.2692	0.2305	0.2496	0.2398	0.2704	0.2384	0.2441	0.2501
Σq_{DBU}	0.7065	0.6558	0.6490	0.6674	0.6663	0.6675	0.6737	0.6838	0.6717	0.6610
Σq_{Bn}	0.2935	0.2635	0.2689	0.2751	0.2657	0.2792	0.2762	0.2833	0.2769	0.2737
CT		0.0808	0.0822	0.0575	0.0681	0.0533	0.0501	0.0329	0.0515	0.0653
Occupancy/au										
σ*(C2−H19)	0.0179	0.0206	0.0218	0.0198	0.0195	0.0202	0.0196	0.0198	0.0224	0.0207
σ*(C4−H23)	0.0178	0.0220	0.0248	0.0211	0.0210	0.0209	0.0208	0.0202	0.0214	
σ*(C6−H25)	0.0198			0.0211		0.0210	0.0214	0.0211	0.0216	
σ*(C9−H31)	0.0138	0.0147	0.0176	0.0172	0.0143	0.0155	0.0152	0.0139	0.0168	0.0170
σ*(C10−H33)	0.0111	0.0103		0.0172	0.0104		0.0109			0.0114
σ*(C12−H35)	0.0146	0.0180	0.0180	0.0180	0.0173	0.0190	0.0201	0.0173	0.0158	0.0189
$E^{(2)}$/kcal mol^{-1}										
ΣLP(Z)→σ*(C2−H19)		1.87	2.03	1.45	1.76	2.08	1.01	1.39	1.11	1.78
ΣLP(Z)→σ*(C4−H23)		2.56	2.54	1.73	2.25	1.36	2.23	0.8	0.31	
ΣLP(Z)→σ*(C6−H25)				0.98		0.31	0.52	0.08	0.81	
ΣLP(Z)→σ*(C9−H31)		0.72	1.48	2.62	1.21	1.53	0.39	0.73	1.07	1.52
ΣLP(Z)→σ*(C10−H33)		0.08		0.06	0.08		0.33			0.20
ΣLP(Z)→σ*(C12−H35)		0.95	2.12	2.51	0.11	3.26	2.77	2.43	0.24	0.72
$\sum E^{(2)}$A unit→ C unit		32.83	30.16	23.42	30.73	23.09	15.49	27.27	14.95	24.05

Z: O or F or N or S atoms in the ([Y_{1-8}] = $[CH_3CO_2]^-$, $[C_6H_5SO_2]^-$, $[C_6H_5SO_3]^-$, $[HCO_3]^-$, $[HSO_4]^-$, $[CF_3CO_2]^-$, $[BF_4]^-$ and $[SCN]^-$) anions.

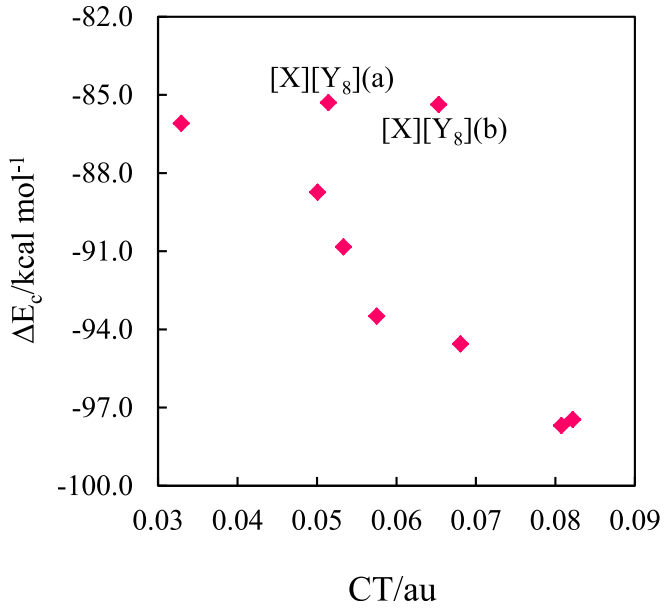

Fig. 11. Correlation between values of CT and corrected interaction energy for[X][Y_{1-8}], Y_{1-8} = $[CH_3CO_2]^-$, $[C_6H_5SO_2]^-$, $[C_6H_5SO_3]^-$, $[HCO_3]^-$, $[HSO_4]^-$, $[CF_3CO_2]^-$, $[BF_4]^-$ and $[SCN]^-$ (a, b)) ILs.

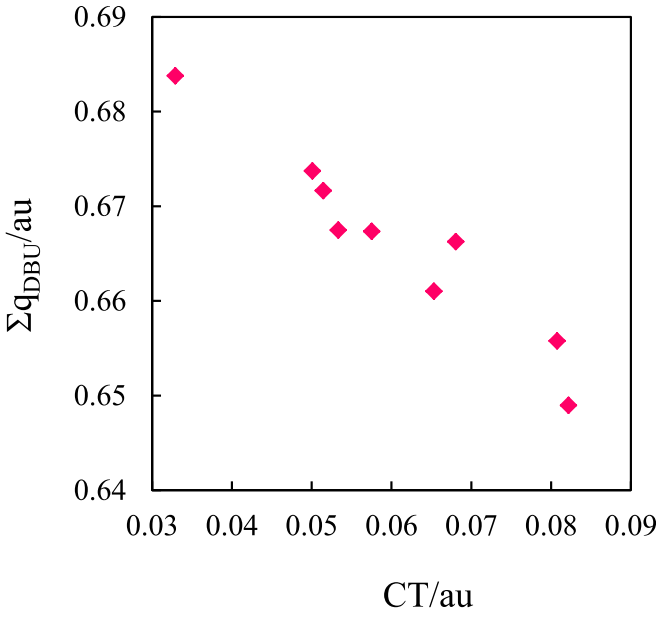

Fig. 12. Correlation between sum of the positive charges carried by DBU rings ($\sum q_{DBU}$) and CT for [X][Y_{1-8}], Y_{1-8} = $[CH_3CO_2]^-$, $[C_6H_5SO_2]^-$, $[C_6H_5SO_3]^-$, $[HCO_3]^-$, $[HSO_4]^-$, $[CF_3CO_2]^-$, $[BF_4]^-$ and $[SCN]^-$ (a, b)) ILs.

detection of the interaction strength. Therefore, values of sign(λ_2) × ρ(r) can be used for detection of interaction types. The negative and positive values of sign(λ_2) × ρ(r) are indicative of attractive (such as dipole-dipole or hydrogen bonding) and nonbonding interactions, respectively. Values near zero specify very weak, van der Waals interactions [74]. The gradient isosurfaces are colored according to the corresponding values of sign(λ_2) × ρ(r). The blue, red and green regions show the H-bonding, strong repulsion interaction and vdW interaction, respectively. Reduced density gradient ($RDG = 1/(2(3\pi^2)^{1/3})|\nabla\rho(r)|/\rho(r)^{4/3}$) is a fundamental dimensionless quantity to describe the deviation from a homogeneous electron distribution. When the quantity RDG is mapped versus signλ_2 × ρ(r), both the nature and strength of the interactions can be categorized.

Fig. 13 show the isosurfaces of sign λ_2 × ρ(r) and Fig. 14 display the RDG versus sign λ_2 × ρ(r) plots for [Bn-DBU][Y_{1-8}], Y_{1-8} = $[CH_3CO_2]^-$, $[PhSO_2]^-$, $[PhSO_3]^-$, $[HCO_3]^-$, $[HSO_4]^-$, $[CF_3CO_2]^-$, $[BF_4]^-$ and $[SCN]^-$ (a, b)) ILs for revealing the non-covalent interactions. The green region between [Bn−DBU]$^+$ cation and the anions indicates the weak vdW interactions in the ILs. The vdW interactions are observed more between the DBU rings of the cation and the anions. The H−bonding interaction takes place between

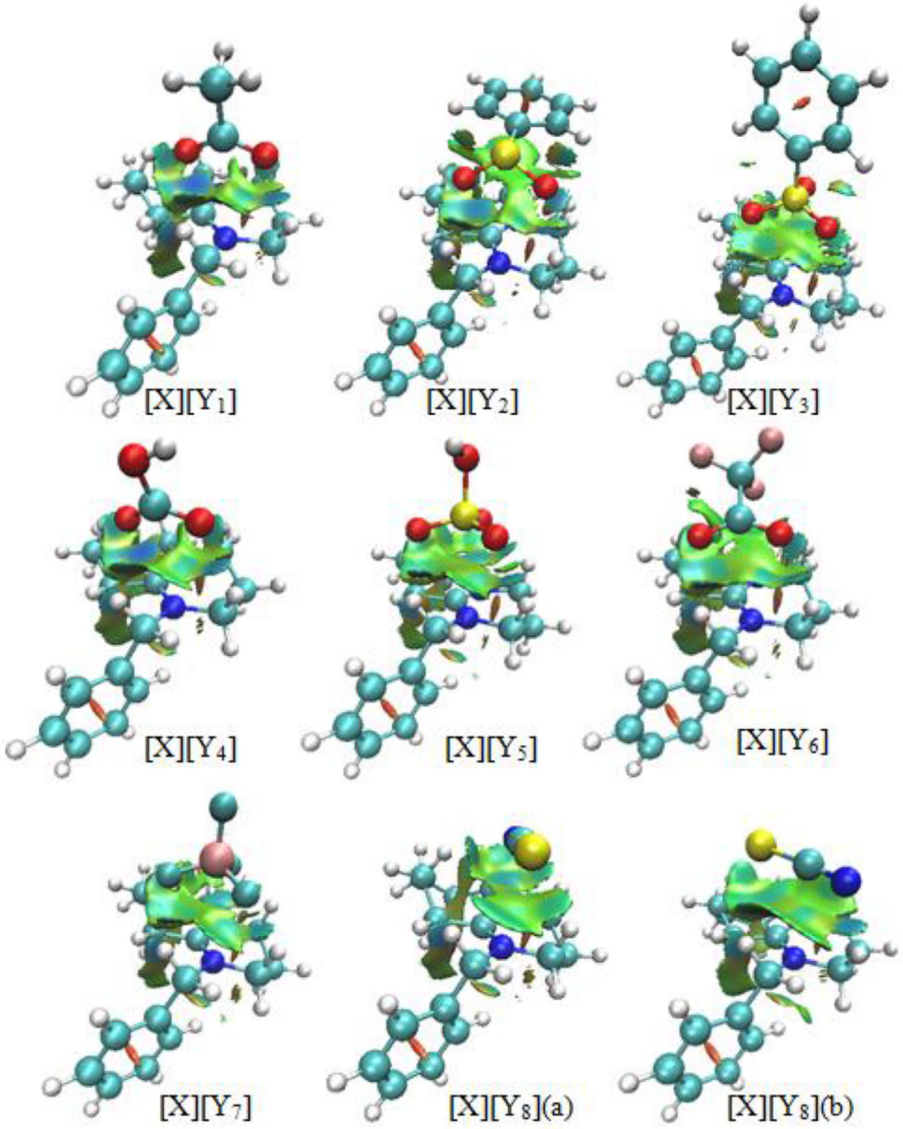

Fig. 13. RDG isosurfaces (s = 0.5 au) for [X][Y_{1-8}], Y_{1-8} = $[CH_3CO_2]^-$, $[C_6H_5SO_2]^-$, $[C_6H_5SO_3]^-$, $[HCO_3]^-$, $[HSO_4]^-$, $[CF_3CO_2]^-$, $[BF_4]^-$ and $[SCN]^-$ (a, b)) ILs. The isosurfaces are colored on a blue-green-red scale according to values of sign(λ_2) × ρ(r), color scale data ranging from −0.03 to 0.03au.

C—H bonds of DBU rings and CH_2 group of benzyl ring of $[Bn-DBU]^+$ cation and O, F, N and S atoms of $CH_3CO_2^-$, $PhSO_2^-$, $PHSO_3^-$, HCO_3^-, HSO_4^-, $CF_3CO_2^-$, BF_4^- and SCN^-anions. Presence of additional isosurface between the phenyl ring of $PhSO_2^-$ anion and the C—H bonds of seven membered DBU ring of the cation *via* cooperative C—H•••π intermolecular interactions in [Bn—DBU][$PhSO_2$] results in its greater stability than six ILs. The color of isosurfaces (darker blue) in [Bn-DBU][CH_3CO_2], [Bn-DBU][$PhSO_2$], [Bn-DBU][HCO_3] reveals that H-bonds are stronger than those found in the other ILs.

As can be seen in Fig. 14 the various spikes exist in the different regions of RDG plot. The locations of these peaks are sensitive to the atom types involved in interaction. RDG plots show that the nature of interactions between the $[Bn-DBU]^+$ cation and the anions are approximately same for [X][Y_{1-8}], Y_{1-8} = $[CH_3CO_2]^-$, $[PhSO_2]^-$, $[PhSO_3]^-$, $[HCO_3]^-$, $[HSO_4]^-$, $[CF_3CO_2]^-$, $[BF_4]^-$ and $[SCN]^-$ (a, b)) ILs. The presence of spikes (−0.04 to ~0 au) corresponding to the H-bonding interactions is in good agreement with HBCP critical points observed in the molecular graphs of ILs.

5. Conclusions

In this study, at first novel ionic liquids based on cation $[Bn-DBU]^+$ cation and $CH_3CO_2^-$, $PhSO_2^-$, $PhSO_3^-$, HCO_3^-, HSO_4^-, $CF_3CO_2^-$, BF_4^- and SCN^- anions were synthesized. Then the effect of various anions on the structural, electronic, energetic and spectroscopic characteristics of [Bn-DBU] based ionic liquids using computational approach based on quantum chemical methods at M06—2X/6—311++G(d,p) level of theory and experimental techniques including ^{1}HNMR, FT-IR and thermogravimetric analyses were evaluated.

The ESP map of $[Bn-DBU]^+$ cation reveals that the positive charge distributions were mostly located on N1, N8, C7 and C—H bonds of the cation. Comparison of the dispersion-corrected interaction energies reveals that the most and least stable structures correspond to [Bn-DBU][$PhSO_2$] and [Bn-DBU][SCN], respectively. The range of the calculated vibrational frequencies of CH_2 group of benzyl of cation, and C═O, S═O, B—F and C≡N groups of anions are in good agreement with the range of experimental values. The results of AIM analysis shows that nature of all

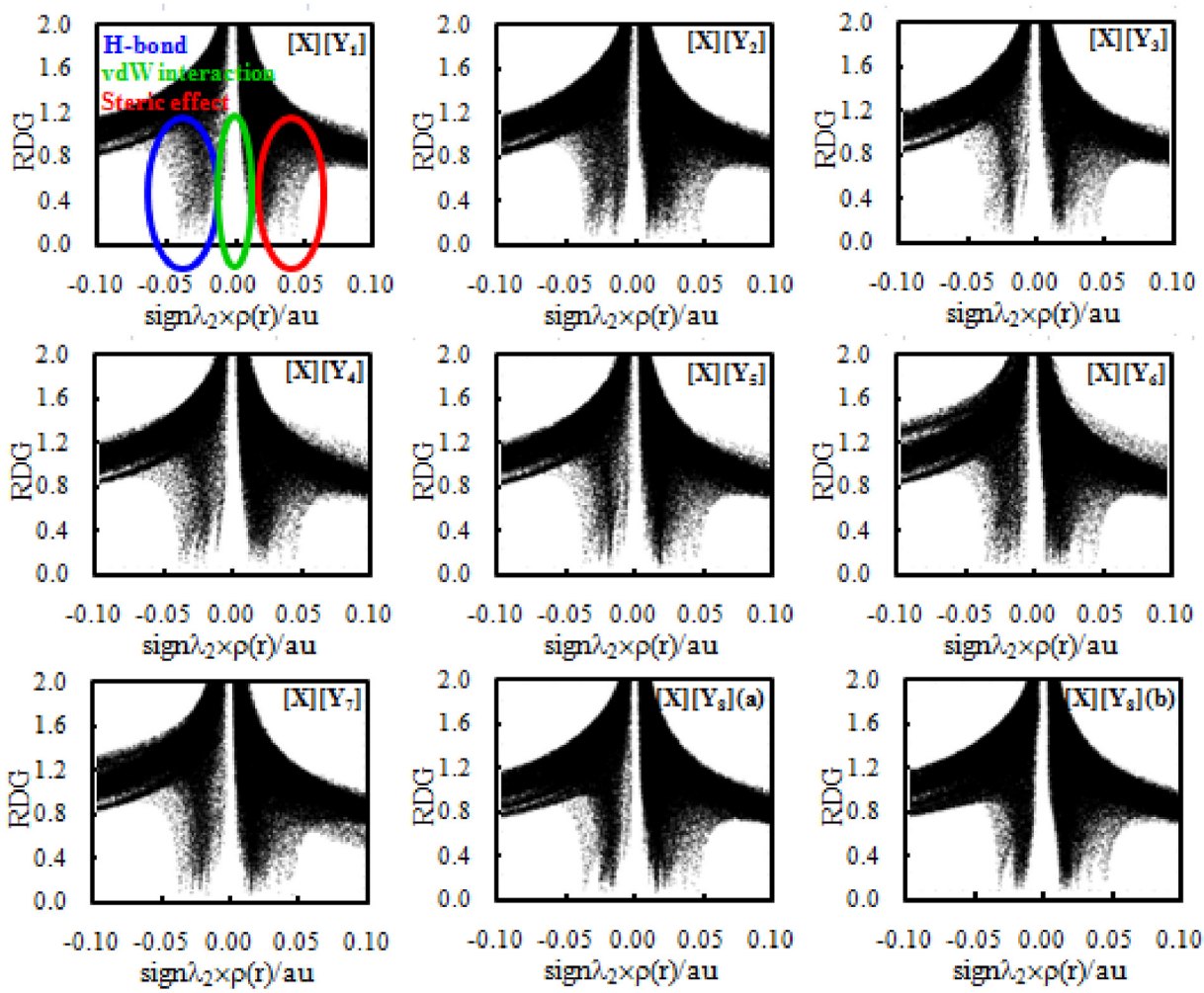

Fig. 14. RDG versus sign $(\lambda_2) \times \rho(r)$ plots for [X][$Y_{1\text{-}8}$], $Y_{1\text{-}8}$ = $[CH_3CO_2]^-$, $[C_6H_5SO_2]^-$, $[C_6H_5SO_3]^-$, $[HCO_3]^-$, $[HSO_4]^-$, $[CF_3CO_2]^-$, $[BF_4]^-$ and $[SCN]^-$ (a, b)) ILs. Favorable interactions appear on the left, unfavorable on the right, and vdW near the zero. The isovalue is set to 0.5 au.

hydrogen bonds in [Bn-DBU][$Y_{1\text{-}8}$] ILs is electrostatic. There is a nearly linear correlation between CT values and interaction energies so that CT value for ILs having the [$Y_{1\text{-}2}$] anions is greater than other ones. The results of NCI analysis are in good agreement with interaction energy, NBO and AIM analyses.

Declaration of competing interest

The all authors declare that they have no conflict of interest.

Appendix A. Supplementary data

Supplementary data to this article can be found online at https://doi.org/10.1016/j.molstruc.2019.127226.

References

[1] P. Wasserscheid, T. Welton, Ionic Liquids in Synthesis, Wiley-VCH, New York, 2003.
[2] R.D. Rogers, K.R. Seddon, S. Volkov, Green Industrial Applications of Ionic Liquids, Springer, New York, 2003.
[3] D.S. Silvester, R.G. Compton, Electrochemistry in room temperature ionic liquids: a review and some possible applications, Z. Phys. Chem. 220 (2006) 1247–1274.
[4] J.P. Hallett, T. Welton, Room-temperature ionic liquids: solvents for synthesis and catalysis, Chem. Rev. 111 (2011) 3508–3576.
[5] S. Zhang, N. Sun, X. He, X. Lu, X. Zhang, Physical properties of ionic liquids: database and evaluation, J. Phys. Chem. Ref. Data 35 (2006) 1475–1517.
[6] Q. Zhang, S. Zhang, Y. Deng, Recent advances in ionic liquid catalysis, Green Chem. 13 (2011) 2619–2637.
[7] R. Ge1, C. Hardacre1, J. Jacquemin, D.W. Rooney, Thermophysical properties of ionic liquids, ACS (Am. Chem. Soc.) Symp. Ser. 1030 (2009) 43–60.
[8] J.M. Esperanc, S.S. Canongia Lopes, N. Jose, M. Tariq, L.M.N.B.F. Santos, J.W. Magee, L.P.N. Rebelo, Volatility of aprotic ionic liquids-A review, J. Chem. Eng. Data 55 (2010) 3–12.
[9] S. Aparicio, M. Atilhan, F. Karadas, Thermophysical properties of pure ionic liquids: review of present situation, Ind. Eng. Chem. Res. 49 (2010) 9580–9595.
[10] J. Carrete, T.M. endez-Morales, M. García, J. Vila, O. Cabeza, L.J. Gallego, L.M. Varela, Thermal conductivity of ionic liquids: a pseudolattice approach, J. Phys. Chem. C 116 (2012) 1265–1273.
[11] M.L. Dietz, Ionic liquids as extraction solvents: where do we stand? Separ. Sci. Technol. 41 (2006) 2047–2063.
[12] C. Chiappe, D. Pieraccini, Ionic liquids: solvent properties and organic reactivity, J. Phys. Org. Chem. 18 (2005) 275–297.
[13] J.D. Holbrey, K.R. Seddon, Ionic liquids, Clean Prod. Process. 1 (1999) 223–236.
[14] T. Welton, Ionic liquids in catalysis, Coord. Chem. Rev. 248 (2004) 2459–2477.
[15] H. Weingrtner, Understanding ionic liquids at the molecular level: facts, problems, and controversies, Angew. Chem. Int. Ed. 47 (2008) 654–670.
[16] J.S. Wilkes, Properties of ionic liquid solvents for catalysis, J. Mol. Catal. A Chem. 214 (2004) 11–17.
[17] N. Ghosh, DBU (1,8-diazabicyclo[5.4.0] undec-7-ene)-A nucleophillic base, Synlett 2004 (2004) 574–575.
[18] M. Baidya, H. Mayr, Nucleophilicities and Carbon Basicities of DBU and DBN. Chem. Commun. (Cambridge, U. K.), 2008, pp. 1792–1794.
[19] B. Yu, H. Zhang, Y. Zhao, S. Chen, J. Xu, L. Hao, Z. Liu, DBU-based ionic-liquid-catalyzed carbonylation of o-phenylenediamines with CO2 to 2-benzimidazolones under solvent-free conditions, ACS Catal. 3 (2013) 2076–2082.
[20] A.-G. Ying, L. Liu, G.-F. Wu, G. Chen, X.-Z. Chen, W.-D. Ye, Aza-Michael addition of aliphatic or aromatic amines to α,β-unsaturated compounds catalyzed by a

DBU-derived ionic liquid under solvent-free conditions, Tetrahedron Lett. 50 (2009) 1653–1657.
[21] S. Mahajan, R. Sharma, R.K. Mahajan, Interactions of new 1, 8-diazabicyclo [5.4. 0] undec-7-ene (DBU) based surface active ionic liquids with amitriptyline hydrochloride: micellization and interfacial studies, Colloids Surf., A 424 (2013) 96–104.
[22] Z. Wang, Z.P. Li, Y.H. Jin, W. Liu, L.H. Jiang, Q.H. Zhang, Organic super base derived ionic liquids based on the TFSI anion: synthesis, characterization, and electrochemical properties, New J. Chem. 41 (2017) 5091–5097.
[23] A.G. Ying, L.M. Wang, L.L. Wang, X.Z. Chen, W.D. Ye, Green and efficient Knoevenagel condensation catalysed by a DBU based ionic liquid in water, J. Chem. Res. 34 (2010) 30–33.
[24] E. Sznti-Pintér, L. Maksa, J. Wouters, B.E. Herman, M. Szécsi, G. Miklee, L. Kollr, R. Skoda-Fldes, Synthesis of 16α-amino-pregnenolone derivatives via ionic liquid-catalyzed aza-Michael addition and their evaluation as C17,20-lyase inhibitors, Steroids 123 (2017) 61–66.
[25] R. Hart, P. Pollet, D.J. Hahne, E. John, V. Llopis-Mestre, V. Blasucci, H. Huttenhower, W. Leitner, C.A. Eckert, C.L. Liotta, Benign coupling of reactions and separations with reversible ionic liquids, Tetrahedron 66 (2010) 1082–1090.
[26] D.J. Heldebrant, P.G. Jessop, C.A. Thomas, C.A. Eckert, C.L. Liotta, The reaction of 1,8-diazabicyclo[5.4.0]undec-7-ene(DBU) with carbon dioxide, J. Org. Chem. 70 (2005) 5335–5338.
[27] V. Singh, D. Singh, R.L. Gardas, Effect of DBU (1, 8-diazobicyclo [5.4.0] undec-7-ene) based protic ionic liquid on the volumetric and ultrasonic properties of ascorbic acid in aqueous solution, Ind. Eng. Chem. Res. 54 (2015) 2237–2245.
[28] E. Privalova, M. Nurmi, M.S. Maranon, E.V. Murzina, P. Maki-Arvela, K. Eranen, D.Y. Murzin, J.-P. Mikkola, CO2 removal with switchable versus classical ionic liquids, Separ. Purif. Technol. 97 (2012) 42–50.
[29] D.J. Heldebrant, C.R. Yonker, P.G. Jessop, L. Phan, Organic liquid CO_2 capture agents with high gravimetric CO_2 capacity, Energy Environ. Sci. 1 (2008) 487–493.
[30] Z. Liu, P. Hu, X. Meng, R. Zhang, H. Yue, C. Xu, Y. Hu, Synthesis and properties of switchable polarity ionic liquids based on organic superbases and fluoroalcohols, Chem. Eng. Sci. 108 (2014) 176–182.
[31] Y. Zhao, B. Yu, Z. Yang, H. Zhang, L. Hao, X. Gao, Z. Liu, A protic ionic liquid catalyzes CO_2 conversion at atmospheric pressure and room temperature: synthesis of quinazoline-2,4-(1H,3H)-diones, Angew. Chem. 126 (2014) 1–5.
[32] P.G. Jessop, Green chemistry: reversible nonpolar-to-polar solvent, Nature 436 (2005) 1102.
[33] C. Samori, C. Torri, G. Samori, D. Fabbri, P. Galletti, F. Guerrini, R. Pistocchi, E. Tagliavini, Extraction of hydrocarbons from microalga Botryococcusbraunii with switchable solvents, Bioresour. Technol. 101 (2010) 3274–3279.
[34] H. Kondo, K. Hatsuda, N. Tano, M. Ito, K. Yun, T. Noguchi, Newly-synthesized Thermally-Stable Ionic Liquids as Friction Modifiers for Carbon-Coated Media, Academic Press, New York, 1992.
[35] K.C. Lethesh, S.N. Shah, M.I. Abdul Mutalib, Synthesis, characterization, and thermophysical properties of 1, 8-diazobicyclo [5.4. 0] undec-7-ene based thiocyanate ionic liquids, J. Chem. Eng. Data 59 (2014) 1788–1795.
[36] K.C. Lethesh, S.N. Shah, M.I. Abdul Mutalib, Synthesis, characterization, physical and thermodynamic properties of diazobicycloundecene based dicyanamide ionic liquids, J. Mol. Liq. 208 (2015) 253–258.
[37] L. Wu, J. Song, B. Zhang, B. Zhou, H. Zhou, H. Fan, Y. Yang, B. Han, Very efficient conversion of glucose to 5-hydroxymethylfurfural in DBU-based ionic liquids with benzenesulfonate anion, Green Chem. 16 (2014) 3935–3941.
[38] E.I. Izgorodina, Z.L. Seeger, D.L.A. Scarborough, S.Y.S. Tan, Quantum chemical methods for the prediction of energetic, physical, and spectroscopic properties of ionic liquids, Chem. Res. 117 (10) (2017) 6696–6754.
[39] H. Roohi, R. Salehi, Molecular interactions in methylimidazolium tetrafluoroborate ionic liquid($[Mim^+][BF_4^-]$): structures, binding energies, topological properties and NMR one- and two bonds spin–spin coupling constants, J. Mol. Liq. 161 (2011) 63–71.
[40] H. Roohi, S. Khyrkhah, Ion-pairs formed in $[Mim^+][N(CN)_2^-]$ ionic liquid: structures, binding energies, NMRSSCCs, volumetric, thermodynamic and topological properties, J. Mol. Liq. 177 (2013) 119–128.
[41] H. Roohi, K. Ghauri, Exploring physicochemical properties of the nanostructured tunable aryl alkyl ionic liquids (TAAILs), J. Mol. Liq. 209 (2015) 14–24.
[42] H. Roohi, K. Ghauri, Influence of various anions and cations on electrochemical andphysicochemical properties of the nanostructured Tunable Aryl Alkyllonic Liquids (TAAILs): a DFT M06-2X study, Thermochim. Acta 639 (2016) 20–40.
[43] H. Roohi, H. Iloukhani, F. Rouhani, Tuning the structural, electronic and electrochemical properties of the 4-methyl-1-phenyl triazoliumbased $[PhMeTAZ][Y_{1\text{-}8}]$ ionic liquids through changing anions: a quantum chemical study, J. Mol. Liq. 240 (2017) 138–151.
[44] H. Roohi, R. Salehi, Molecular engineering of the electronic, structural, and electrochemical properties of nanostructured1-methyl-4-phenyl 1,2,4 triazolium-based $[PhMTZ][X_{1-10}]$ ionicliquids through anionic changing, Ionics 24 (2018) 483–504.
[45] Y. Zhao, D.G. Truhlar, The M06 suite of density functionals for main group thermochemistry, thermochemical kinetics, noncovalent interactions, excited states, and transition elements: two new functionals and systematic testing of four M06-class functionals and 12 other functionals, Theor. Chem. Acc. 120 (2006) 215–241.
[46] Y. Zhao, D.G. Truhlar, Density functionals with broad applicability in chemistry, Acc. Chem. Res. 41 (2008) 157–167.
[47] A.D. McLean, G.S. Chandler, Contracted Gaussian basis sets for molecular calculations. I. Second row atoms, Z=11–18, J. Chem. Phys. 72 (1980) 5639–5648.
[48] S.F. Boys, F. Bernardi, The calculation of small molecular interactions by the differences of separate total energies.Some procedures with reduced errors, J. At. Mol. Phys. 19 (1970) 553–566.
[49] M.J. Frisch, G.W. Trucks, H.B. Schlegel, G.E. Scuseria, M.A. Robb, J.R. Cheeseman, G. Scalmani, V. Barone, B. Mennucci, G.A. Petersson, H. Nakatsuji, M. Caricato, X. Li, H.P. Hratchian, A.F. Izmaylov, J. Bloino, G. Zheng, J.L. Sonnenberg, M. Hada, M. Ehara, K. Toyota, R. Fukuda, J. Hasegawa, M. Ishida, T. Nakajima, Y. Honda, O. Kitao, H. Nakai, T. Vreven, J.A. Montgomery, J.E. Peralta Jr., F. Ogliaro, M. Bearpark, J.J. Heyd, E. Brothers, K.N. Kudin, V.N. Staroverov, R. Kobayashi, J. Normand, K. Raghavachari, A. Rendell, J.C. Burant, S.S. Iyengar, J. Tomasi, M. Cossi, N. Rega, J.M. Millam, M. Klene, J.E. Knox, J.B. Cross, V. Bakken, C. Adamo, J. Jaramillo, R. Gomperts, R.E. Stratmann, O. Yazyev, A.J. Austin, R. Cammi, C. Pomelli, J.W. Ochterski, R.L. Martin, K. Morokuma, V.G. Zakrzewski, G.A. Voth, P. Salvador, J.J. Dannenberg, S. Dapprich, A.D. Daniels, O. Farkas, J.B. Foresman, J.V. Ortiz, J. Cioslowski, D.J. Fox, Gaussian 09, Revision A.02, Inc., Gaussian, Wallingford, CT, 2009.
[50] P. Politzer, D.G. Truhlar, Chemical Applications of Atomic and Molecular Electrostatic Potentials: Reactivity, Structure, Scattering, and Energetics of Organic, Inorganic, and Biological Systems, Springer, New York, 2013.
[51] T. Lu, F.W. Chen, Multiwfn: a multifunctional wavefunction analyzer, J. Comput. Chem. 33 (2012) 580–592.
[52] A.E. Reed, L.A. Curtiss, F. Weinhold, Intermolecular interactions from a natural bond orbital, donor-acceptor viewpoint, Chem. Rev. 88 (1988) 899–926.
[53] E.D. Glendening, A.E. Reed, J.E. Carpenter, F.A. Weinhold, NBO, Version 3.1, Department of Chemistry, University of California-Irvine, Irvine, CA, 1995.
[54] F. Biegler-König, J. Schönbohm, D. Bayles, AIM2000-A program to analyze and visualize atoms in molecules, J. Comput. Chem. 22 (2001) 545–560.
[55] F.M. Bickelhaupt, E.J. Baerends, Kohn-Sham density functional theory: predicting and understanding chemistry, Rev. Comput. Chem. 15 (2000) 1–86.
[56] G. TeVelde, F.M. Bickelhaupt, E.J. Baerends, S.J.A. Van Gisbergen, C. Fonseca Guerra, J.G. Snijders T. Ziegler, Chemistry with ADF, J. Comput. Chem. 22 (2001) 931–967.
[57] ADF 2009.01; theoretical chemistry, V.U., SCM, Amsterdam, The Netherlands, http://www.scm.com.
[58] E.R. Johnson, S. Keinan, P. Mori-Sanchez, J. Contreras-García, A.J. Cohen, W. Yang, Revealing noncovalent interactions, J. Am. Chem. Soc. 132 (2010) 6498–6506.
[59] J. Contreras-García, E.R. Johnson, S. Keinan, R. Chaudret, J. Philip Piquemal, D.N. Beratan, W. Yang, NCIPLOT: a program for plotting noncovalent interaction regions, J. Chem. Theory Comput. 7 (2011) 625–632.
[60] W. Humphrey, A. Dalke, K. Schulten, VMD: visual molecular dynamics, J. Mol. Graph. 14 (1996) 33–38.
[61] M.C. Kroon, W. Buijs, C.J. Peters, G.-J. Witkamp, Quantum chemical aided prediction of the thermal decomposition mechanisms and temperatures of ionic liquids, Thermochim. Acta 465 (2007) 40–47.
[62] H. Tokuda, K. Hayamizu, K. Ishii, M.A.B.H. Susan, M. Watanabe, Physicochemical properties and structures of room temperature ionic liquids, 1. Variation of anionic species, J. Phys. Chem. B 108 (2004) 16593–16600.
[63] A. Diop, A.H. Bouazza, C. Daneault, D. Montplaisir, New ionic liquid for the dissolution of lignin, Bioresour 8 (2013) 4270–4282.
[64] J. Nowicki, M. Muszynski, S. Gryglewicz, Novel basic ionic liquids from cyclic guanidines and amidines-New catalysts for transesterification of oleochemicals, J. Chem. Technol. Biotechnol. 89 (2013) 48–55.
[65] M.S. Miran, H. Kinoshita, T. Yasuda, M.A.B.H. Susan, M. Watanabe, Physicochemical properties determined by ΔpKa for protic ionic liquids based on an organic super-strong base with various Brønsted acids, Phys. Chem. Chem. Phys. 14 (2012) 5178–5186.
[66] N. Mohan, C.H. Suresh, A. Kumar, S.R. Gadre, Molecular electrostatics for probing lone pair-π interactions, Phys. Chem. Chem. Phys. 15 (2013) 18401–18409.
[67] A. Kumar, S.R. Gadre, N. Mohan, C.H. Suresh, Lone Pairs: an electrostatic viewpoint, J. Phys. Chem. A 118 (2014) 526–532.
[68] S.R. Gadre, A. Kumar, Bonding and reactivity patterns from electrostatic landscapes of molecules, J. Chem. Sci. 128 (2016) 1519–1526.
[69] U. Koch, P.L.A. Popelier, Characterization of C-H-0 Hydrogen Bonds on the basis of the charge density, J. Phys. Chem. 99 (1995) 9747–9754.
[70] P.L.A. Popelier, Characterization of a dihydrogen bond on the basis of the electron density, J. Phys. Chem. A 102 (1998) 1873–1878.
[71] P. Hobza, Z. Havlas, Blue-shifting hydrogen bonds, J. Chem. Rev. 100 (2000) 4253–4264.
[72] P. Hobza, V. Spirko, H.L. Selzle, E.W. Schlag, Anti-hydrogen bond in the benzene dimer and other carbon proton donor complexes, J. Phys. Chem. A 102 (1998) 2501–2504.
[73] A.E. Reed, L.A. Curtiss, F. Weinhold, Intermolecular interactions from a natural bond orbital, donor-acceptor viewpoint, Chem. Rev. 88 (1998) 899–926.
[74] E.R. Johnson, S. Keinan, P. Mori-Sánchez, J. Contreras-García, A.J. Cohen, W. Yang, Revealing noncovalent interactions, J. Am. Chem. Soc. 132 (18) (2010) 6498–6506.